This is a preprint, the final version is subject to change, of the American Mineralogist (MSA)
Cite as Authors (Year) Title. American Mineralogist, in press.
DOI: https://doi.org/10.2138/am-2018-6352

REVISION 1

Immiscible sulfide melts in primitive oceanic magmas: evidence and implications from picrite lavas (Eastern Kamchatka, Russia)

DMITRY P. SAVELYEV[1], VADIM S. KAMENETSKY[2,3,*], LEONID V. DANYUSHEVSKY[2], ROMAN E. BOTCHARNIKOV[4], MAYA B. KAMENETSKY[2], JUNG-WOO PARK[5], MAXIM V. PORTNYAGIN[6,7], PAUL OLIN[2], STEPAN P. KRASHENINNIKOV[7], FOLKMAR HAUFF[6], AND MICHAEL E. ZELENSKI[3]

[1]Institute of Volcanology and Seismology FEB RAS, Petropavlovsk-Kamchatsky 683006, Russia

[2]Earth Sciences and CODES, University of Tasmania, Hobart, Tasmania 7001, Australia

[3]Institute of Experimental Mineralogy RAS, Chernogolovka 142432, Russia

[4]Institut für Mineralogie, Leibniz Universität, Hannover 30167, Germany

[5]School of Earth and Environmental Sciences & Research Institute of Oceanography, Seoul National University, Seoul 08826, South Korea

[6]GEOMAR Helmholtz Center for Ocean Research, Kiel 24148, Germany

[7]V.I. Vernadsky Institute of Geochemistry and Analytical Chemistry, Moscow 119991, Russia

* E-mail: Dima.Kamenetsky@utas.edu.au

ABSTRACT

Silicate-sulfide liquid immiscibility in mantle-derived magmas has important control on the budget of siderophile and chalcophile metals, and is considered to be instrumental in the origin orthomagmatic sulfide deposits. Data on primitive sulfide melts in natural samples, even those

representing most voluminous magmatism in oceanic rifts, are very scarce due to the small size and poor preservation of incipient sulfide melt globules. Here we present the first detailed report of the crystallized sulfides melts in the oceanic picrites of the (presumably) Cretaceous age Kamchatsky Mys ophiolite complex in Eastern Kamchatka (Far East Russia). Sulfide melts are present in three forms; 1) as inclusions in olivine (87.1–89.6 mol% Fo), 2) interstitial to the groundmass minerals (clinopyroxene, plagioclase and Ti-magnetite) of studied picrites, and 3) as daughter phases in silicate melt inclusions hosted by olivine and Cr-spinel phenocrysts. The sulfide melt inclusions in olivine and the groundmass of studied rocks are composed of several sulfide phases that correspond to the monosulfide (Fe–Ni; *Mss*) and intermediate (Fe–Cu–Ni; *Iss*) solid solutions. Several <0.5 μm Pd–Sn, Pt– and Au–Ag phases are recorded within the matrix sulfides, commonly along phase boundaries and fractures. Major elements (S, Fe, Cu, Ni, Co), platinum group elements (PGE) and gold analyzed in the homogenized olivine-hosted sulfide melt inclusions, and phases identified in the matrix sulfides record the range of magmatic sulfide compositions. The most primitive sulfide liquids are notably enriched in Ni and Cu ((Ni+Cu)/Fe, at. > 0.5), continuously evolve with crystallization of (e.g., increasing Cu/Ni and Au/PGE) and demonstrate metal fractionation between *Mss* and *Iss*. Although the compositional systematics found in this study are consistent with those previously recorded, the compositions of individual sulfide phases are strongly affected by the noble metal (PGE, Au) 'nuggets' that exsolve at subsolidus temperatures and form during serpentinization of the rocks. We conclude that the budget of noble metals in the studied picrites is controlled by sulfides, but the abundances of Pt and Au are influenced by mobility in post-magmatic alteration. Our data can be also used for modelling sulfide saturation at crustal pressures and understanding behavior of the noble metals in primitive oceanic magmas.

Keywords: Silicate-sulfide immiscibility, mid-ocean ridge magmatism, picrite, olivine, sulfide melt, platinum-group elements

INTRODUCTION

Orthomagmatic models assume that many types of economic mineralization hosted in igneous rocks implicitly relate to magmas and magma–derived fluids (e.g., Burnham, 1998; Hedenquist and Lowenstern, 1994; Naldrett, 2004 and references therein). The origin of 'mineralizing fluids' is often linked to liquid immiscibility (unmixing) in parental silicate magmas (Roedder, 1992). The compositional divergence between unmixed phases can be extreme, and even though the physical amount of the new segregated phase may be small, it can extract, accumulate and transport large amounts of trace and rare elements (Roedder, 1992;

Veksler et al., 2012). Small amounts and transient, reactive qualities of immiscible phases render the understanding of their intrinsic compositions through the study of natural samples extremely difficult (e.g., Kamenetsky and Kamenetsky, 2010). The research problem persists with experimental and theoretical modelling being too simplistic to account for all physical and chemical variables in control of magmatic immiscibility.

Immiscibility between silicate and sulfide melts that occurs in a variety of mantle-derived magmas is believed to be a starting point in the formation of Cu–Ni sulfide deposits with platinum group elements (hereafter, PGE) (e.g., Naldrett, 2004). Unfortunately, the majority of continental rocks that host such deposits do not fit general criteria for primary/primitive melts (i.e., they feature <8 wt% MgO and the absence of high–forsteritic olivine phenocrysts). Even in the case of rare high–Mg rocks with primitive olivine in some large igneous provinces on continents (see review in Kamenetsky et al., 2017), a record of the early sulfide immiscibility is yet to be discovered. In contrast to continental magmas, sulfide globules in phenocrysts and glasses at mid-ocean ridge basalts (MORB) have been documented since the underwater samples became available in the 1960's (e.g., Czamanske and Moore, 1977; Francis, 1990; Kanehira et al., 1973; MacLean, 1977; Mathez, 1976; Moore and Calc, 1971; Peach et al., 1990). These studies provided first insights into occurrence of silicate–sulfide unmixing in shallow plumbing systems during crystallization and eruption, but lacked specific details about the liquidus assemblage and compositions at the onset of immiscibility.

After a long period of quiescence the research on sulfide globules in MORB has been recently resurrected (e.g., Kamenetsky et al., 2013; Keith et al., 2017; Patten et al., 2012; Patten et al., 2013; Yang et al., 2014), however, scarcity of modern data still limits understanding of compositions of incipient sulfide melts, their compositional evolution with fractionation, and

metal partitioning between immiscible silicate and sulfide liquids. This paper is the first comprehensive report of several types of immiscible sulfide liquids in primitive oceanic magmas.

GEOLOGICAL SETTING AND SAMPLES

The Kamchatsky Mys (hereafter, "KM") ophiolite complex in the easternmost Kamchatka Peninsula (Far East Russia) is renowned for its present-day tectonic position at the junction of the Kuril-Kamchatka arc, Aleutian arc and the inferred starting point of the Hawaiian-Emperor seamount chain (Fig. 1). Several studies have suggested that sedimentary rocks (e.g., shales, limestones, cherts), igneous rocks (e.g., lavas, hyaloclastites, dykes and gabbros) and mantle peridotites in the ophiolite assemblage are possibly different in age, and hence belong to different geodynamic settings (e.g., Zinkevich et al., 1985; Fedorchuk et al., 1989). The alternative explanation assumes mid–Cretaceous (Albian – Cenomanian) age (Palechek et al., 2010) for most rocks, and that the KM ophiolite represents magmatism and sedimentation in the former Kula–Pacific spreading center (Khotin and Shapiro, 2006; Portnyagin et al., 2005; Saveliev, 2003). The age and compositions of the ophiolite is consistent with the interpretation that it is the earliest expression of interaction of the Hawaiian "plume" and paleo-spreading center (Batanova et al., 2014; Portnyagin et al., 2009; Portnyagin et al., 2008; Portnyagin et al., 2005; Saveliev, 2003).

The volcanic rocks in the upper part of the KM ophiolite are basalts belonging to the tholeiitic, sub-alkaline and alkaline series (e.g., Fedorchuk, 1992; Portnyagin et al., 2008; Portnyagin et al., 2005; Saveliev, 2003). The enriched tholeiites are geochemically similar to those from the neighboring Meiji and Detroit Seamounts (Portnyagin et al., 2008), whereas ultra-depleted melt compositions contributed to N-MORB tholeiitic basalts (Portnyagin et al., 2009).

The olivine-phyric (picrite) rocks with magmatic sulfides reported here have been recently discovered in the serpentinite mélange that borders the ultramafic massif of Mt. Soldatskaya (Fig. 1; Savelyev, 2014), where ~1.5 m picrite boulders were found trailing in a small outcrop (~400 x 250 m) among debris of peridotites. The samples represent cumulates of euhedral olivine (40-50 %; Table 1) and rare plagioclase and Cr-spinel crystals set in a crypto- to holocrystalline (doleritic) matrix, composed of clinopyroxene– plagioclase– Ti-magnetite aggregates. In some varieties dendritic radial (sheaf-like) growth of groundmass minerals and altered interstitial glass are indicative of relatively fast cooling.

Olivine phenocrysts ranging in size up to 2-3 mm are moderately fractured and serpentinized along fractures and grain boundaries. Olivine is dominantly primitive (Fo_{87-90}), does not show chemical zoning except for more Fe-rich thin (~200 μm) outer rims, and has trace element systematics typical for MORB olivine (i.e., 0.25–0.35 wt% NiO, 0.26–0.30wt% CaO, 0.14–0.18 wt% MnO; Savelyev, 2014). Reddish-brown Cr-spinel, present as phenocrysts (up to 0.4 mm) and inclusions (<0.15 mm) in olivine, is characteristically Mg- and Al-rich (68–76 mol% Mg#, 19–40 mol% Cr#) and Ti-poor (0.25–0.43 wt% TiO_2; Savelyev, 2014) and thus compositionally similar to MORB spinel. Both olivine and Cr-spinel phenocrysts contain crystallized inclusions of the silicate and sulfide melts.

The large abundance of olivine phenocrysts in the studied picrites is responsible for the high MgO contents (24–28 wt%) and low abundances of non-olivine major elements (8–9 wt% Al_2O_3, 5–6 wt% CaO; Table 1) in the whole rock compositions. In addition to mineral compositions, the MORB-like geochemical characteristics of parental melts for the studied picrites are expressed in the contents and ratios of incompatible trace elements (e.g., La/Sm = 1.5–2, Gd/Yb = 1.3–1.6, Nb/La = 0.8–1.4). The origin from a MORB-type depleted mantle is

further confirmed by unradiogenic $^{87}Sr/^{86}Sr$ (0.70243), radiogenic $^{143}Nd/^{144}Nd$ (0.51315) and moderately radiogenic Pb ($^{206}Pb/^{204}Pb$=18.90, $^{207}Pb/^{204}Pb$=15.50, $^{208}Pb/^{204}Pb$=38.20) isotope compositions (Appendix 1[1]).

METHODS

Sample preparation

Sulfides were extracted from ~ 20 kg of rocks. The rocks were crushed and sieved (<0.2 mm, 0.2-0.5 mm and 0.5-2 mm). A heavy fraction was then separated by panning in water. Olivine grains were hand-picked from the heavy fraction 0.5-2 mm and examined under a binocular microscope for sulfide inclusions. Rock fragments (0.2 to 2 mm) from the heavy fraction were further separated into non-magnetic and magnetic fractions. The latter fraction yielded sulfide grains > 0.1 mm that were picked by hand, mounted in epoxy resin and polished. Sulfides were inspected in reflected light using the optical microscope, photographed, and selected for analytical work.

Electron microscope and electron microprobe

Backscattered electron (BSE) imaging and energy dispersive X-ray spectrometry (EDS) were performed on a Hitachi SU-70 Schottky field emission SEM fitted with an Oxford AZtec XMax 80 silicon drift detector EDS system at 15 kV at the University of Tasmania, and a VEGA 3 (Tescan, Czech Republic) scanning electron microscope with an energy-dispersive spectrometer X-Max 50 at the Institute of Volcanology and Seismology (Petropavlovsk-Kamchatsky, Russia). Sulfur, Fe, Ni and Cu were calibrated on celestite, hematite, nickel silicide and cuprite (Astimex Standards Ltd, Toronto, Canada) using the K x-ray series for quantification. To correct for changes in the beam current between calibration and sample data acquisition, the cobalt Ka peak intensity was measured on pure cobalt metal at the start of each session.

Electron microprobe analysis (EMPA) using a Cameca SX100 electron microprobe (Institut für Mineralogy, Leibniz Universität Hannover, Germany) determined major element concentrations in sulfides. To minimize effects of small-scale heterogeneity caused by phase segregation (or exsolution) during cooling, sulfide samples were analyzed with the electron beam defocused to 20 μm. Iron, S and Si were analyzed using 15 keV accelerating voltage, 15 nA beam current and 10 sec accumulation time. Nickel and Cu were analyzed using 15 keV, 100 nA beam current and 30 sec accumulation time. When possible, larger phases were analyzed in several locations to test for homogeneity. Calibration of the analyses was performed using a number of standards (Fe on Fe_2O_3, S on FeS_2, Si on $CaSiO_3$, Ni on NiO, Cu on Cu metal).

Laser ablation ICPMS

Laser ablation inductively-coupled plasma mass spectrometry (LA–ICP–MS) analyses of sulfides were carried out at CODES Analytical Laboratories, University of Tasmania. The instrumentation was an ASI RESOLution-LR-S155 laser microprobe equipped with a Coherent Compex-Pro 193 nm Ar-F excimer laser, coupled to an Agilent 7700x quadrupole ICP-MS. A laser beam size of 29 μm was used with a pulse rate of 5 Hz and a fluence of 2.7 J/cm^2 to drill holes into sulfide samples and standard materials. Ablation was performed in a He atmosphere flowing at ~0.35 L/min. The ablated aerosol was mixed with Ar (1.05 L/min) as a transport gas, before exiting the small volume cell. Tuning was performed to minimize oxide production (<0.15 % ThO/Th) and maximize sensitivity for the mid and high mass isotopes. The following isotopes measured were: ^{34}S, ^{57}Fe, ^{59}Co, ^{60}Ni, ^{63}Cu, ^{66}Zn, ^{99}Ru, ^{101}Ru, ^{103}Rh, ^{105}Pd, ^{106}Pd, ^{111}Cd, ^{185}Re, ^{189}Os, ^{193}Ir, ^{195}Pt and ^{197}Au. Dwell time was 5 ms for S, 10 ms for Fe, Co, Ni, Cu and Zn and 20 ms for all other elements, resulting in a total sweep time of 0.275 sec. Total acquisition time for each analysis was 90 seconds, consisting of a 30 second gas background and a 60 second ablation signal. Quantification was performed following the standard methods (Košler, 2001; Longerich et al., 1996). Calibration involved STDGL3 (Danyushevsky et al., 2011), NIS3 (Gilbert et al., 2013) and Po724-T (Sylvester et al., 2005) reference materials, and Fe as the internal standard element. Instrumental drift was corrected by regular (at least hourly) analyses of references materials across the analytical session. Due to the unknown bulk composition of the sulfide inclusions, quantification involved normalization to 100 wt% total. Corrections for base metal-argide interferences are required for the quantification of Ru, Rh and Pd concentrations by LA-ICP-MS techniques (Guillong et al., 2011; Sylvester, 2001). The analysis of magmatic sulfides has the potential to form

argide interferences of $^{61}Ni^{40}Ar$ on ^{101}Ru, $^{59}Co^{40}Ar$ on ^{99}Ru, $^{63}Cu^{40}Ar$ on ^{103}Rh, $^{65}Cu^{40}Ar$ on ^{105}Pd, and $^{66}Zn^{40}Ar$ on ^{106}Pd. For the quantification of Ru, Rh and Pd, the extent of base metal-argide production was determined by ablating pure Ni, Cu, Zn and Co metals and a correction factor applied to the results. All ^{106}Pd results were corrected for isobaric interference from ^{106}Cd which was monitored by recording signal on ^{111}Cd.

Whole rock analyses

Two rock samples were analyzed for major, trace and platinum-group elements in three research institutes in South Korea. First, they were powdered in an agate mill at the Korea Polar Research Institute (KOPRI). A 0.95 g split of the powder was mixed with 9.5 g of Li-tetraborate and <0.03 g of Li-bromide. The mixture was fused in a platinum crucible in an open furnace at 1100℃ for 15 min. The fused disks were analyzed on a S8 TIGER (Bruker, Germany) XRF at the National Center for Inter-university Research Facilities, Seoul National University (SNU).

Trace element contents were determined by LA-ICP-MS at the Korea Basic Science Institute. A 0.5 g split of the sample powder was mixed with 1.0 g of lithium tetraborate and 0.5 g of lithium metaborate. The mixture was fused at 1000°C for 30 minutes using a Katanax K2 Prime Electric Fusion Machine at KOPRI. The fused glass disks were analyzed by a LA-ICP-MS system, consisting of a Photon-Machines EXCITE193 excimer laser and a Thermo Scientific iCAP-Q ICP-MS. The analyses were performed at the laser pulse rate of 10 Hz, beam size of 135 μm, and energy density of ~ 10 J/cm^2. A NIST 612 glass standard was used as an external standard for calculating the trace element contents with Si contents obtained by XRF analysis. In order to check the reproducibility and precision of the analyses we performed multiple analyses of the reference material BHVO-2 (n=7) and BCR-2G (n=2). The reproducibility calculated using relative standard deviation (1σ) was mostly less than 5 % for all elements.

Whole-rock PGE contents were measured using the Ni sulfide fire assay-isotope dilution method by Park et al. (2012). A 2.5 g split of the powder was thoroughly mixed with 0.25 g of Ni, 0.125 g of S and 2.5 g of sodium borax. An enriched PGE spike solution (^{99}Ru, ^{105}Pd, ^{191}Ir and ^{195}Pt) was added to the mixture. The spiked powder was dried at 100℃ for 1 hour and fused in porcelain Coors^{TM} crucibles in a preheated open furnace at 1150℃ for 30 minutes. The reducing conditions were provided by flowing N_2 gas into the furnace and adding ~0.1 g of cereal flour into the second outer crucible. After quenching, Ni-sulfide beads were recovered and dissolved in 6M HCl. The solution was then filtered through a Millipore 0.45 μm cellulose membrane filter to collect the PGE-bearing minerals. The filter paper containing the PGE minerals was digested in 4 ml of aqua regia, and after complete digestion, the solutions were dried down to <0.1 ml and diluted with 2% HNO_3. The solutions were analyzed for PGE isotopes on an Elan 6100 quadrupole ICP-MS system at the Seoul National University. Potential molecular interferences on the analyzed isotopes by Ni, Cu, Zn, Co, Hf, Mo, Zr and Ta argides or oxides were monitored and the effects of the interferences were subtracted using measured oxide (0.2–1.9%) and argide production rates (0.002–0.01%). The interference correction is <0.2% for all PGE, except for Ru for which the correction is 3-4%. Concentrations of Ir, Ru, Pt, Pd and Re were determined by isotope dilution using the $^{191}Ir/^{193}Ir$, $^{99}Ru/^{101}Ru$, $^{191}Ir/^{193}Ir$, $^{195}Pt/^{194}Pt$, $^{105}Pd/^{108}Pd$ and $^{185}Re/^{187}Re$ ratios, respectively. Concentrations of Rh were obtained using the method by Meisel et al. (2003) and Park et al. (2012), where count rates of ^{103}Rh and ^{106}Pd are used, assuming that the loss of Rh during the analytical procedure was similar to the loss of Pd. Average procedural blanks measured by sample-free analyses (n=4) were 22±6 pg Ir, 36±25 pg Ru, 9±4 pg Rh, 268±58 pg Pt, and 295±87 pg Pd. The method detection limits (MDL) were taken to be three standard deviations of the procedural blanks. MDLs for 2.5 g samples are 8 ppt for Ir, 30 ppt for Ru, 11 ppt for Rh, 69 ppt for Pt and 105 ppt for Pd. The accuracy and precision of the analyses were assessed by multiple analyses (n=4) of reference material TDB-1. The reproducibility is 4-11% for Ru, Pt and Pd, 17% for Ir and 29% for Rh. The measured TDB-1 values were consistent with published values.

RESULTS

Sulfide occurrences

Three types of sulfide appearance are recorded in the KM olivine-phyric rocks Figs. 2-4): 1) masses in the plagioclase-clinopyroxene-magnetite groundmass, 2) inclusions in olivine and Cr-spinel and 3) daughter phases in silicate melt inclusions hosted by phenocrysts.

Sulfide in the groundmass (hereafter, "*matrix sulfide*") is represented by relatively large grains (~ 0.1 mm, up to 0.6 mm) with highly variable shapes. Areal measurements of matrix sulfide grains in 18 thin sections (~ 4 cm^2 each) and S abundances in whole rocks (~ 0.05 wt.%, Table 1) indicate ~ 0.1 % sulfide is present in the studied rocks, however, the sizes and distributions of matrix sulfides are highly irregular. The shapes and textures of matrix sulfides reflect cooling and crystallization of both sulfide liquid and host silicate liquid, and an overwhelming number of matrix sulfides have had their surfaces "shaped" by other groundmass minerals (Fig. 2). The host silicate liquid was interstitial to earlier olivine and Cr-spinel phenocrysts, and crystallized well-formed, interlocking clinopyroxene, plagioclase and Ti-magnetite groundmass with irregularly shaped, partially flat-walled interstices into which matrix sulfides crystallized. Accordingly, matrix sulfides (once trapped liquid droplets) are rarely spherical (or circular to oval in cross-section), and only so if entrapped by plagioclase and Ti-magnetite (Figs. 2c and 2e). More often, matrix sulfides show curvature at contacts with olivine phenocrysts (Figs. 2b and 8a). Matrix sulfides are observed squished and even pierced through by neighboring silicate and oxide phases (Figs. 2d–2g) and wrapped around earlier formed Cr-spinel (Fig. 2a). The observed scalloped edges, lobate surfaces and tubular embayments of the matrix sulfides could result from interaction between a molten sulfide and crystallizing silicate-oxide groundmass. Most matrix sulfides bear signs of alteration (e.g., cracking, oxidation).

Sulfide inclusions in olivine and Cr-spinel phenocrysts represent a second type of sulfide melt in the samples (Figs. 3 and 7). The spherical and, rarely, cylindrical inclusions found in a very small number of olivine grains (~ 0.7%) are commonly singular (rarely 2-3 per olivine grain) and relatively small (< 100 μm). Phenocryst-hosted sulfides are undoubtedly entrapped sulfide melts (e.g., Ackermand et al., 1998; Czamanske and Moore, 1977; Francis, 1990;

241 Gurenko et al., 1987; Kamenetsky and Kamenetsky, 2010), and thus they are labelled "*sulfide*
242 *melt inclusions*" in this study.

243 The third type of sulfide occurs as small globules (commonly < 1 μm) hosted in partially
244 crystalline silicate melt inclusions in olivine and Cr-spinel (Fig. 4). They are interpreted as a
245 daughter phase that formed during cooling in relation to the so-called Fe loss process, caused by
246 post-entrapment crystallization and re-equilibration with the host mineral (Danyushevsky et al.,
247 2002). A number of daughter sulfide globules in a given melt inclusion is hard to estimate due to
248 opacity of the crystalline silicate and host Cr-spinel, but the number and size of individual
249 globules are inversely correlated. A given section of any melt inclusion may contain several
250 equally sized globules (0.3-0.4 μm; Fig. 4d) or a larger number of much smaller globules (<0.1
251 μm). Co-entrapment of sulfide and silicate liquids could also be the case, where sulfides
252 (typically > 5 μm) are volumetrically disproportional to enclosing silicate melt, and develop
253 scalloped embayments and flattened edges at contacts with silicates (Figs. 4c and 4f). No
254 correlation was found between the size and composition of sulfide globules and their position
255 relative to the host inclusion walls, vapor bubble(s) or daughter pyroxene crystals (Figs. 4b and
256 4e).

257 **Sulfide phase and major element compositions**

258 Matrix sulfides and sulfide melt inclusions are composed of at least four coarse phases that
259 can be recognized in reflected light and backscattered electrons. A light-grey, euhedral Fe-oxide
260 phase, most likely magnetite, is minor and can be absent in a given section, especially in sulfide
261 melt inclusions. The phase boundaries between intimately intergrown sulfide phases are distinct,
262 and can be both straight and curvilinear (Figs. 8, 12, 13). The proportion between sulfides

263 revealed in any given exposure is highly variable, which does not permit confident calculation of
264 the bulk composition.

265 The matrix sulfides analyzed *in situ* by EMPA (Appendix 2[1]) belong to two main
266 compositional populations that conform to their optical colors. One population is virtually Cu-
267 free (< 2 wt% Cu) and characterized by variable Fe and Ni contents (Fig. 5a, Table 2, Appendix
268 3[1]) and (Fe+Ni)/S ratios (at.) that vary between 1.0 and 1.14 and are negatively correlated with
269 Fe. The second population has high Cu abundances (22-34 wt%), narrow range in Fe (30-37
270 wt%), large range in Ni/Cu (0.04-0.50, at.; Fig. 5a, Table 2, Appendix 3[1]) and metal/S ratios,
271 varying between 1.04 and 1.23 (at.) and are positively correlated with Fe. No stoichiometric
272 minerals were confidently identified among the matrix sulfides, except Ni-poor pyrrhotite. Thus,
273 we tentatively assigned widely used terms monosulfide solid solution (*Mss*) and intermediate
274 solid solution (*Iss*) to Fe-Ni and Fe-Cu-Ni phases, respectively. The same two compositional
275 populations are clearly recognizable in the majority of LA–ICP–MS analyses (Figs. 5b and 8,
276 Appendix 3[1]).

277 The phases in the sulfide melt inclusions are coarse and compositionally similar to those in
278 matrix sulfides (Figs. 3b and 3c). In order to estimate bulk compositions, six sulfide melt
279 inclusions in olivine phenocrysts (87.1-89.6 mol% Fo) were homogenized in a vertical furnace at
280 the V.I. Vernadsky Institute of Geochemistry (Moscow, Russia). They were heated to 1355 °C
281 for 5 min at 1 atm of CO_2:H_2 gas mixture corresponding to the QFM oxygen buffer and then
282 quenched in water. The resulting textures are fine-grained with different sulfide phases
283 intermixed on a much smaller scale than in nature (Fig. 7). The heated inclusions show a good
284 match between the compositions at exposed surfaces and bulk compositions analyzed by SEM-
285 EDS and LA–ICP–MS methods, respectively (Fig. 6a). The major element compositions of all

six homogenized inclusions are very similar, but resemble neither *Mss* nor *Iss*; instead, they likely represent a mixture of these two end-member sulfide phases in roughly equal proportions (Fig. 5). The sulfide melt inclusions demonstrate conspicuous changes with fractionation of the silicate melt, namely positive correlation between Ni, Ni/Fe and Ni/Cu and Fo content of the host olivine (Fig. 6b, Table 2). One of the homogenized sulfide inclusions is cylindrical and distinctively larger than other five spherical globules (Fig. 7c), but not different in major element composition (Table 2, #3).

Fifty-nine daughter sulfide globules (0.5-1 μm) in 35 silicate melt inclusions hosted by Cr-spinel (Figs. 4d and 4e) were studied by SEM-EDS. Twenty-nine inclusions contained only one exposed sulfide globule, whereas from 3 to 8 sulfides globules were exposed and analyzed in other inclusions. Most compositions are Cu-free or Cu-poor (< 5 at%), and belong to the *Mss* endmember with variable Ni/Fe (0-0.93, average 0.19 ± 0.22, at.), whereas Cu-bearing sulfides (> 10 at%) are rare (Fig. 5c). The compositions of daughter sulfides in a given melt inclusion are highly variable (Fig. 5c) and show no correspondence with the size and position of globules.

Sulfide trace and minor element compositions

Thirty-nine matrix sulfides and six sulfide melt inclusions were analyzed using the LA-ICP-MS method (79 spots) to determine concentrations and distribution of noble metals (PGE, Au and Re) and trace metals (Zn and Cd). The selection of grains of matrix sulfides was based on occurrence of both *Mss* and *Iss* phases on polished surface and their size large enough (> 30-40 μm) for the laser ablation analysis. Major elements of the sulfide matrix (Fe, Ni, Co, Cu and S) were also measured together with trace elements, and used for data reduction and to monitoring the phase compositions. The behavior of the elements during analysis was registered with time-resolved laser ablation spectra (Figs. 7 and 8), used to determine if sulfides are

homogeneous "down hole" (i.e. constant element ratios in the ablated volume), and if they contain noble-metal phases (hereafter, *nuggets*) large enough to be recorded. The majority of single point analyses demonstrate homogeneous major element compositions, however several analytical spots returned "mixed" compositions (i.e. *Mss* + *Iss*), encountered within the analyzed volume (Fig. 5b; also see Fig. 8A "mt3-5b"). Importantly, all sulfide melt inclusions appeared homogeneous below their exposed surface (Fig. 7) and show good correspondence between the surface SEM-EDS and the volume LA-ICP-MS (Fig. 6a).

All elements analyzed in the sulfide melt inclusions are above the detection limit (Table 2) and correspond well (except Pt) to the average composition of the analyzed matrix sulfides (Figs. 9, 10 and 11b). The time-resolved laser ablation spectra of the sulfide melt inclusions are smooth and bear no evidence of nuggets (Fig. 7). Six sulfide melt inclusions show contents of PGE and Au that are unexpectedly variable (Figs. 10, 11a and 14, Table 2), given their similar major element compositions and limited compositional range of their host olivine. It is worth mentioning that one unusually PGE-enriched composition belongs to the inclusion that is largest and, unlike other inclusions, cylindrical (#3 in Table 2 and Fig. 7c). Even if this anomalous composition is excluded, the PGE contents in five smaller and spherical sulfide globules are still highly variable (by a factor of 2.5 for Rh to 13.8 for Ir) and positively correlated with Fo content of the host olivine (Figs. 10 and 11a, Table 2).

The chalcophile and noble metal compositions of the KM matrix sulfides encompass the range of the sulfide melt inclusions, but are even more fluctuating for both *Mss* and *Iss* phases (Figs. 9 and 10, Appendix 3[1]). The chalcophile elements Zn and Cd concentrate in the Cu-rich sulfide (*Iss*, Figs. 9a and 9b), whereas Ni-rich sulfide (*Mss*) is more enriched in Re (Fig. 10b). Cobalt, which has chalcophile and siderophile affinities, partitions strongly to *Mss*, however, it

correlates positively with Ni in both *Mss* and *Iss* phases of the matrix sulfides (Fig. 9c). Some analyzed PGE (e.g., Os, Ir and Pt) appear to be below detection limits (~ 0.005-0.01 ppm) in a large number of analyses (Appendix 3[1]). Based on this detection limits, the overall compositional variation is at least two orders of magnitude (Fig. 10). The iridium-group PGE (IPGE) correlate exceptionally well with each other in both *Mss* and *Iss* of the matrix sulfides and sulfide melt inclusions, but are 3-4 times more abundant in *Mss*.(Fig. 10). In contrast, the platinum-group PGE (PPGE) and Au show different systematics to each other and IPGE. For example, the average abundances of Rh are similar in *Mss*, *Iss* and sulfide melt inclusions (~ 0.2 ppm), covariate with IPGE only in *Mss* and melt inclusions, but remains relatively constant in *Iss* (Figs. 10d and 10e, Table 2). Palladium and gold show weak and strong preference, respectively, for *Iss*, however, they are not correlated with each other and other PGE in either of studied phases (Fig. 10f, Table 2). As mentioned above, Pt is often undetectable in the matrix sulfides, especially *Iss* (Fig. 10h), which is in contrast to its high and variable abundances in the sulfide melt inclusions (0.44-7.03 ppm, Table 2). Moreover, Pt contents in the matrix sulfides do not correlate with other PGE and demonstrate a pronounced negative anomaly relative to normalized (primitive mantle (PM) using values from McDonough and Sun (1995) concentrations of neighboring Rh and Pd (Fig. 11b).

Compositions of the sulfide melt inclusions and the average matrix sulfide from the KM picrite are similar in terms of major elements (Fig. 5b), IPGE and Re (Figs. 9–11). The average matrix sulfide is notably more enriched in Zn, Rh and Pd compared to the average sulfide melt inclusion, but is relatively depleted in Co, Cd, Au and especially Pt (Figs. 9–11). For comparing PGE abundances in sulfides and whole rock analyses we have assumed that the matrix sulfide is largely responsible for the overall PGE budget of the rocks. The amount of sulfide present, based

on counting statistics and sulfur abundances in whole rocks, is ~ 0.1%. Using this value, the measured PGE contents are multiplied by 10^3 and show good agreement with the sulfide PGE pattern (Fig. 11b), therefore, reinforcing our original assumption.

The time-resolved laser ablation spectra recorded the presence of dominantly Pd- or/and Au-bearing nuggets of variable size in 57% of analytical spots (Fig. 8). These nuggets, previously observed by SEM-EDS on polished surfaces of matrix sulfides, are described in more detail below.

Noble-metal nuggets in matrix sulfides

Noble metal nuggets are common in all matrix sulfide grains, with occasionally 10-15 particles observed on a given surface (~ 500 μm^2; Fig. 12). They usually occur on phase boundaries and in cracks, and range significantly in size (< 0.05 to 1 μm) even in the same field of view (Fig. 12). The small size of nuggets hampers accurate determination of compositions by energy-dispersive spectrometry because the analytical volume (at an accelerating voltage of 15-17 keV, specimen density ~ 4.5 g/cc) is around 1–1.2 μm across, exceeding the size of most nuggets. Semi-quantitative compositions of nuggets ≥ 0.3 μm can be estimated by subtracting matrix elements (Fe, Ni, Cu, and S) from the analyses. In most cases the neighboring nuggets show diverse compositions and morphology (Fig. 12). There is no correlation between the compositions of the sulfide matrix (i.e. *Mss* or *Iss*) and included nuggets. Palladium is by far the most abundant element occurring with Sn as a Pd-Sn alloy with variable Pd/Sn (1.7-2.5), but Pd_2Sn (paolovite) is the most common. Alloys of Au and Ag mixed in different proportions (0.5-2.7 at.), as well as pure Au, is the second dominant phase. Typically both types of alloys (Pd-Sn and Au-Ag) occur in close vicinity to each other (Fig. 12), which is also seen in the time-

resolved laser ablation spectra (Fig. 8). Sometimes Ag-free gold contains minor Pd (3-14 %), whereas low quantity of Zn and Pt maybe present in Au-Ag alloys.

In addition to common Pd-Sn and Au-Ag nuggets in matrix sulfides we record phases that contain Pt-As ± Ni-As ± Au ± Ag ±Te, Bi. They are larger (up to 2-3 μm) and occur along and at intersection of cracks, at the contacts of sulfides with the alteration silicates (chlorite, serpentine) and within the latter (Fig. 13). Typically they appear as a chain-like "decoration" of the sulfide grain boundaries and even take the form of micro-veinlets (Fig. 13). Sperrylite ($PtAs_2$), Au-Ag alloys, maucherite ($Ni_{11}As_8$) and $Pt_3(As,Te,Bi)_7$ dominate the population.

DISCUSSION

Early sulfide saturation in oceanic magmas

Petrography and chemical data suggest that the MORB-type magmas from Kamchatsky Mys achieved the sulfide saturation. The common occurrence of sulfides in the pyroxene-plagioclase-Ti-magnetite groundmass and their irregular, often deformed shapes (Fig. 2) imply that these sulfides were in a liquid or plastic state at the time of eruption and were affected by groundmass minerals growing around and through them. A close similarity between the average composition of matrix sulfides and sulfide globules included in olivine phenocrysts from same samples (Figs. 5b, 9 and 10) suggests that studied sulfides belong to the same population of immiscible melts.

Our data are consistent with the records of omnipresent sulfide globules in the Atlantic and Pacific basalts and glasses (e.g., Czamanske and Moore, 1977; Kanehira et al., 1973; MacLean, 1977; Mathez, 1976; Moore and Calc, 1971) and reconfirm sulfide saturation of common MORB melts during crystallization (e.g., Haughton et al., 1974; Mathez, 1976). Moreover, sulfide melt inclusions in primitive olivine in this (Fig. 3, 7; Table 2) and other

400 studies (e.g., Kamenetsky and Kamenetsky, 2010) should be considered as the earliest
401 manifestation of the silicate-sulfide immiscibility in oceanic magmas. Such records are
402 exceptionally rare, but provide the strongest support for sulfide immiscibility in the crust without
403 the requirement of magma contamination by sulfur-enriched crustal material and/or extensive
404 fractionation, advocated in some studies (see review in Naldrett, 2004).

405 **Composition of incipient sulfide melts**

406 The homogenized sulfide melt inclusions in primitive olivine (Fig. 7) provide a snapshot
407 of natural sulfide liquids at the onset of immiscibility. Once entrapped in olivine the sulfide melt
408 inclusions are effectively insulated from further interactions with their parental silicate melts,
409 and thus they are considered to maintain their original composition in terms of major and trace
410 elements, including noble metals.

411 In contrast to constraints from theoretical and experimental modelling (e.g., Naldrett,
412 2004; Zhang, 2015), the olivine-hosted sulfide globules in this and other studies (e.g.,
413 Ackermand et al., 2007; Czamanske and Moore, 1977; Francis, 1990; Zelenski et al., 2017) are
414 not pure FeS, but contain substantial amounts of other metals (Fig. 5; (Ni+Cu)/Fe = 0.47-0.59).
415 Similar Ni- and Cu-rich compositions of primitive sulfide melts are reported for globules in
416 MORB glasses (e.g., Kamenetsky et al., 2013; Keith et al., 2017; Patten et al., 2012; Peach et al.,
417 1990; Yang et al., 2014). In particular, there is a good match between the major element
418 compositions of KM sulfide melt inclusions and high Ni/Cu sulfide globules in the FAMOUS
419 glass ALV 526-1 (Fig. 5a). Noteworthy, a significant range in the individual compositions of 22
420 sulfide globules in a single glass ALV 526-1 (Ni/Cu = 0.6-1.7 (at) as in Fig. 5a; 1220-1870 ppm
421 Co, 2-23 ppm Au, 35-1472 ppb Ir; Peach et al., 1990) clearly demonstrates that sulfide melts can
422 be compositionally heterogeneous on a very local scale (i.e., within the same silicate liquid).

Likewise, small-scale disequilibrium is demonstrated by variable compositions of daughter sulfide globules in single melt inclusions in our study (Figs. 4 and 5c). On the other hand, "*a state close to chemical equilibrium with the host magma*" was proposed for individual sulfide globules in seven MORB glasses (Patten et al., 2013), based on corresponding compositions in terms of Ni, Cu and Co abundances. The results by Patten et al. (2013) and compositional relationships between incipient sulfide melts and host olivine (Figs. 6b and 11a) show that the evolution of MORB sulfide liquids is characterized by decreasing Ni/Cu. This mirrors the effects of olivine crystallization (i.e., Ni intake) in parental magmas (e.g., Kamenetsky and Eggins, 2012). On the other hand, compositions of individual sulfide globules hosted by the same glass (Fig. 5a; Peach et al., 1990) strongly imply their derivation from compositionally different batches of magma and incomplete re-equilibration with the melt that transported them to the surface (e.g., Yang et al., 2014). Additional insights into equilibration of incipient sulfide melts can be provided by noble metal compositions of sulfide melt inclusions and matrix sulfides.

It is expected that PGE abundances will decrease with fractionation of olivine and Cr-spinel and concomitant separation of immiscible sulfide liquids. The olivine-hosted sulfide melts in our study, excluding one anomalously enriched composition (#3 in Table 2, Fig. 7c), demonstrate a four-fold to seven-fold decrease in PPGE and IPGE, respectively, and co-variation of PGE with olivine Fo and sulfide Ni/Cu (Figs. 11a and 14). However, anticipated smooth and (sub) parallel trends for normalized compositions are not observed for these early sulfide melts (Fig. 11a). Moreover, the correlations between PGE observed in our large dataset (Fig. 10) are not mimicked by dependence of PGE ratios (except Pd/Os, Rh/Ru and Rh/Os) on the compositions of sulfide matrix (Ni/Cu) and host olivine (Fig. 14, Table 2). Unlike total PGE abundances, Au contents seem to be unrelated to olivine and sulfide fractionation, however,

Au/PGE ratios are remarkably consistent (Fig. 14, also see Mungall and Brenan, 2014). It is noteworthy that each trend of the fractionation-driven increase in Au/PGE ratios, except Au/Os, has at least one outlier represented by sulfide melt inclusions #2 (Au/Ru), #3 (Au/Pd), and #4 (Au/Pt, Au/Ir) in Table 2. Five analyzed sulfide melts have moderately to high fractionated PGE except the inclusion #5 (c.f., PPGE/IPGE = 3.0–6.4 and 0.90; Table 2, Fig. 14).

Although the overall compatible behavior of PGE in magmatic fractionation is confirmed, we are concerned with 1) the large magnitude of PGE variation observed in a small number of studied primitive sulfide melts in olivine of restricted composition $Fo_{87.1\text{-}89.6}$; and 2) the lack of correlation between the degree of fractionation and PGE ratios (except very few shown on Fig. 14). Additionally, at least four out of six studied sulfide melt inclusions have abundances of certain noble metals that do not fit anticipated fractionation trends and are at odds with other PGE. The above concerns are highly pertinent to the crystallization of noble metal phases in primitive magmas (e.g., Kamenetsky et al., 2015; Zelenski et al., 2016; Zelenski et al., 2017 and references therein). Such phases may increase the availability of PGE+Au to concurrent sulfide melts through direct entrapment or have the opposite effect by reducing the noble metal budget of the silicate melt undergoing sulfide immiscibility.

Effects of crystallization and alteration of sulfide melts

The shapes, textures, and compositions of matrix sulfide in the KM olivine-phyric rocks record a prolonged and complex process starting with solidification of the sulfide liquid as both Fe-Ni and Fe-Cu-Ni solid solutions, followed by solid-state recrystallization and transformation, and ultimately modifications by alteration and weathering. The shapes of the matrix sulfides (Fig. 2) conform to an essentially liquid state at the time of olivine accumulation. Bulk metal contents of the matrix sulfides do not seem to influence their shape and texture. Although a few

compositions might represent Ni-bearing pyrrhotite, other in-situ analyses do not correspond to stoichiometric minerals (Fig. 5a). The two principal components of the matrix sulfides represent *Mss* and *Iss* that are recorded in MORB sulfide globules worldwide (e.g., Keith et al., 2017; Patten et al., 2012; Patten et al., 2013; Yang et al., 2014 and references therein). Our observations are not conclusive about the order of crystallization/solidification of *Mss, Iss* and small magnetite grains in the KM matrix sulfides.

Only estimates of phase compositions are possible due to the heterogeneity of matrix sulfides. As they represent former sulfide melts cogenetic with primitive olivine, which makes the bulk of picrite rocks, their compositions are envisaged as also relatively primitive. This is supported by the close similarity between the average matrix sulfide (*Mss* and *Iss* in 39 grains) and sulfide melt inclusions in terms of major and chalcophile trace elements and IPGE (Figs. 9, 10 and 11b). The average matrix sulfide is slightly enriched in Pd compared to most sulfide melt inclusions, but depleted in Pt (c.f., Pt/Pd 0.11 vs 0.7-3.1) and Au (c.f., Au/Pd 0.6 vs 1.0-7.1). This relative depletion of matrix sulfides in Pt and Au could be caused by pervasive low-temperature alteration of KM rocks. Preferential low-temperature extraction of Pt and Au from matrix sulfides, mobility and subsequent precipitation is confirmed by occurrence of minerals and alloys of Pt and Au in the vicinity of sulfides (Fig. 13). Occurrences of Pt and Ni arsenides and Au-Ag alloys in chain-like aggregates along fractures in sulfides, at sulfide-silicate interfaces, and in hydrous silicates (Fig. 13) support their non-magmatic origin. Low-temperature crystallization of PGE-bearing phases in the rocks containing magmatic sulfides and Cr-spinel is not unusual (e.g., Barkov and Fleet, 2004).

The effects of alteration on *Mss* and *Iss* are expected to be selective and different for certain elements. Therefore, the predicted partitioning of IPGE into Fe-Ni and PPGE into Fe-Cu

492 sulfide phases (e.g., Ballhaus et al., 2001) cannot be fully evaluated in our study. However, if
493 disturbance of magmatic abundances of IPGE by alteration was insignificant, these elements do
494 show preference for *Mss*, but are highly variable in both *Mss* and *Iss* (Fig. 10). Average contents
495 of Rh are similar in both phases, however, in contrast to nearly constant Rh in *Iss*, Rh in *Mss*
496 varies over two orders of magnitude and correlates with IPGE (Fig. 10). Chalcophile elements
497 Zn and Cd show strong preference for *Iss*, whereas Co and Re are concentrated in *Mss*. The
498 anticipated partitioning of Pd into *Iss* is not confirmed in our study, as both sulfide phases in
499 matrix sulfides can be extremely depleted or enriched in Pd (0.01 to ~ 30 ppm; Fig. 10, Table 2,
500 Appendix 2[1]). Furthermore, the presence of abundant micro- to nanoscale Pd-Sn alloys in both
501 *Mss* and *Iss* (Figs. 8 and 12) makes understanding of Pd partitioning even more difficult.
502 Finally, the PGE systematics in the KM picrites is comparable to those of sulfide melt
503 inclusions and matrix sulfides, except Pt (Fig. 11b). The comparison is based on the petrographic
504 estimate of 0.1% sulfide and demonstrates that the whole rock PGE budget is dominated by PGE
505 in matrix sulfides. The deficit of Pt in matrix sulfides compared to whole rock and olivine-hosted
506 inclusions (Fig. 13) can be explained by formation of hydrothermal Pt-rich phases during
507 serpentinization.

508 ## IMPLICATIONS

509 Our study of the MORB-type picrite rocks from Kamchatka demonstrate that magmatic
510 sulfides in volcanic rocks and associated silicate and oxide minerals and their silicate melt
511 inclusions is a natural laboratory for understanding silicate-sulfide immiscibility and related
512 partitioning of noble and chalcophile metals. Our data and observations imply that magmatic
513 sulfide liquids undergoing cooling and solidification separate into Fe-Ni and Fe-Cu-Ni phases
514 that have significant compositional ranges in terms of metal/metal, metal/sulfur and PGE ratios.

These two principal sulfide phases not only share the trace and noble metals dissolved in the parental sulfide liquid, but are also responsible for in-situ fractionation of these elements. The established partitioning of IPGE and PPGE+Au into *M*ss and *I*ss, respectively, should be further studied using matrix sulfides from modern MORB. We draw attention to redistribution of noble metals in magmatic sulfides during their crystallization (i.e. formation of "nuggets") and low-temperature alteration of their host rocks. Our results suggest that the latter process affected the matrix sulfides and was responsible for leaching some noble metals and their deposition as hydrothermal phases of Pt, Au and Ag. Thus any 'orthomagmatic' sulfide deposit, composed of stoichiometric phases (pyrrhotite, pentlandite and chalcopyrite) and having local enrichments and depletions in certain noble metals should not be considered 'primary magmatic'. Instead, further research into the origin of accumulations of Fe-Ni-Cu sulfides with high PGE contents in magmatic rocks may pay more attention to post-solidus modifications of original sulfide liquids including hydrothermal mobility and redistribution of the noble metals.

ACKNOWLEDGEMENTS

We are grateful to T. M. Philosofova, K. Goemann and S. Feig for help with electron microscopy. Two anonymous reviewers and the guest editor Raúl O.C. Fonseca are acknowledged for critically evaluating this manuscript. Support from the DFG grant Bo2941/4-1 to REB and Korea Government Ministry of Science, ICP and Future Planning grant NRF-2015R1C1A1A01054101 was provided to JWP. This study was funded by the Russian Science Foundation grant #16-17-10145 to VSK and MEZ.

REFERENCES CITED

Ackermand, D., Hekinian, R., and Stoffers, P. (1998) Magmatic sulfides and oxides in volcanic rocks from the Pitcairn hotspot (South Pacific). Mineralogy and Petrology, 61, 149-162.

Ackermand, D., Hekinian, R., and Stoffers, R. (2007) Mineralogy of magmatic sulfides and transition metal oxides from lavas of the Pitcairn Hotspot and the Pacific Antarctic Ridge. Neues Jahrbuch Fur Mineralogie-Abhandlungen, 184, 77-94.

Ballhaus, C., Tredoux, M., and Späth, A. (2001) Phase relations in the Fe-Ni-Cu-PGE-S system at magmatic temperature and application to massive sulphide ores of the Sudbury igneous complex. Journal of Petrology, 42, 1911-1926.

Barkov, A.Y., and Fleet, M.E. (2004) An unusual association of hydrothermal platinum-group minerals from the Imandra layered complex, Kola Peninsula, northwestern Russia. Canadian Mineralogist, 42, 455-467.

Batanova, V.G., Lyaskovskaya, Z.E., Savelieva, G.N., and Sobolev, A.V. (2014) Peridotites from the Kamchatsky Mys: Evidence of oceanic mantle melting near a hotspot. Russian Geology and Geophysics, 55, 1395-1403.

Burnham, C.W. (1998) Magmas and hydrothermal fluids. In H.L. Barnes, Ed. Geochemistry of Hydrothermal Ore Deposits, p. 63-123. J.Wiley & Sons, New York.

Czamanske, G.K., and Moore, J.G. (1977) Composition and phase chemistry of sulfide globules in basalt from the Mid-Atlantic ridge rift valley near 37^{o} N lat. Geological Society of America Bulletin, 88, 587-599.

Danyushevsky, L., Robinson, P., Gilbert, S., Norman, M., Large, R., McGoldrick, P., and Shelley, M. (2011) Routine quantitative multi-element analysis of sulphide minerals by laser ablation ICP-MS: Standard development and consideration of matrix effects. Geochemistry: Exploration, Environment, Analysis, 11, 51-60.

Danyushevsky, L.V., McNeill, A.W., and Sobolev, A.V. (2002) Experimental and petrological studies of melt inclusions in phenocrysts from mantle-derived magmas: an overview of techniques, advantages and complications. Chemical Geology, 183, 5-24.

Fedorchuk, A.V. (1992) Oceanic and back-arc basin remnants within accretionary complexes: geological and geochemical evidence from eastern Kamchatka. Ofioliti, 17, 219-242.

Francis, R.D. (1990) Sulfide globules in mid-ocean ridge basalts (MORB), and the effect of oxygen abundance in Fe-S-O liquids on the ability of those liquids to partition metals from MORB and komatiite magmas. Chemical Geology, 85, 199-213.

Gilbert, S., Danyushevsky, L., Robinson, P., Wohlgemuth-Ueberwasser, C., Pearson, N., Savard, D., Norman, M., and Hanley, J. (2013) A comparative study of five reference materials and the Lombard meteorite for the determination of the platinum-group elements and gold by LA-ICP-MS. Geostandards and Geoanalytical Research, 37, 51-64.

Guillong, M., Danyushevsky, L., Walle, M., and Raveggi, M. (2011) The effect of quadrupole ICPMS interface and ion lens design on argide formation. Implications for LA-ICPMS analysis of PGE's in geological samples. Journal of Analytical Atomic Spectrometry, 26, 1401-1407.

Gurenko, A.A., Poliakov, A.I., and Kononkova, N.N. (1987) Immiscible sulfide segregations in minerals of early crystallization stages of basaltic rock series. Doklady Akademii Nauk SSSR, 293, 439-443.

Haughton, D.R., Roeder, P.L., and Skinner, B.J. (1974) Solubility of sulfur in mafic magmas. Economic Geology, 69, 541-567.

Hedenquist, J.W., and Lowenstern, J.B. (1994) The role of magmas in the formation of hydrothermal ore deposits. Nature, 370, 519-527.

582 Kamenetsky, V.S., and Eggins, S.M. (2012) Systematics of metals, metalloids, and volatiles in
583 MORB melts: effects of partial melting, crystal fractionation and degassing (a case study
584 of Macquarie Island glasses). Chemical Geology, 302-303, 76-86.
585 Kamenetsky, V.S., and Kamenetsky, M.B. (2010) Magmatic fluids immiscible with silicate
586 melts: examples from inclusions in phenocrysts and glasses, and implications for magma
587 evolution and metal transport. Geofluids, 10, 293–311.
588 Kamenetsky, V.S., Maas, R., Fonseca, R.O.C., Ballhaus, C., Heuser, A., Brauns, M., Norman,
589 M.D., Woodhead, J.D., Rodemann, T., Kuzmin, D.V., and Bonatti, E. (2013) Noble
590 metals potential of sulfide-saturated melts from the subcontinental lithosphere. Geology,
591 41, 575-578.
592 Kamenetsky, V.S., Maas, R., Kamenetsky, M.B., Yaxley, G.M., Ehrig, K., Zellmer, G.F.,
593 Bindeman, I.N., Sobolev, A.V., Kuzmin, D.V., Ivanov, A.V., Woodhead, J., and
594 Schilling, J.-G. (2017) Multiple mantle sources of continental magmatism: Insights from
595 "high-Ti" picrites of Karoo and other large igneous provinces. Chemical Geology, 455,
596 22-31.
597 Kamenetsky, V.S., Park, J.-W., Mungall, J.E., Pushkarev, E.V., Ivanov, A.V., Kamenetsky,
598 M.B., and Yaxley, G.M. (2015) Crystallization of platinum-group minerals from silicate
599 melts: Evidence from Cr-spinel–hosted inclusions in volcanic rocks. Geology, 43, 903-
600 906.
601 Kanehira, K., Yui, S., Sakai, H., and Sasaki, A. (1973) Sulphide globules and sulphur isotope
602 ratios in the abyssal tholeiite from the Mid-Atlantic Ridge near 30^{o}N latitude.
603 Geochemical Journal, 7, 89-96.
604 Keith, M., Haase, K.M., Klemd, R., Schwarz-Schampera, U., and Franke, H. (2017) Systematic
605 variations in magmatic sulphide chemistry from mid-ocean ridges, back-arc basins and
606 island arcs. Chemical Geology, 451, 67-77.
607 Khotin, M.Y., and Shapiro, M.N. (2006) Ophiolites of the Kamchatsky Mys Peninsula, eastern
608 Kamchatka: Structure, composition, and geodynamic setting. Geotectonics, 40, 297-320.
609 Košler, J. (2001) Laser-ablation ICPMS study of metamorphic minerals and processes. In P.J.
610 Sylvester, Ed. Laser-ablation in the earth sciences: principles and application, 29, p. 185–
611 202. Mineralogical Association of Canada.
612 Longerich, H.P., Jackson, S.E., and Gunther, D. (1996) Laser ablation inductively coupled
613 plasma mass spectrometric transient signal data acquisition and analyte concentration
614 calculation. Journal of Analytical Atomic Spectrometry, 11, 899-904.
615 MacLean, W.H. (1977) Sulfides in Leg 37 drill core from Mid-Atlantic Ridge. Canadian Journal
616 of Earth Sciences, 14, 674-683.
617 Mathez, E.A. (1976) Sulfur solubility and magmatic sulfides in submarine basalt glass. J
618 Geophys Res, 81, 4269-4276.
619 McDonough, W.F., and Sun, S.-s. (1995) The composition of the Earth. Chemical Geology, 120,
620 223-253.
621 Meisel, T., Fellner, N., and Moser, J. (2003) A simple procedure for the determination of
622 platinum group elements and rhenium (Ru, Rh, Pd, Re, Os, Ir and Pt) using ID-ICP-MS
623 with an inexpensive on-line matrix separation in geological and environmental materials.
624 Journal of Analytical Atomic Spectrometry, 18, 720-726.
625 Moore, J.G., and Calc, L. (1971) Sulfide spherules in vesicles of dredged pillow basalt.
626 American Mineralogist, 56, 476-488.

Mungall, J.E., and Brenan, J.M. (2014) Partitioning of platinum-group elements and Au between sulfide liquid and basalt and the origins of mantle-crust fractionation of the chalcophile elements. Geochimica Et Cosmochimica Acta, 125, 265-289.

Naldrett, A.J. (2004) Magmatic Sulfide Deposits: Geology, geochemistry and exploration. Springer-Verlag, Berlin Heidelberg.

Palechek, T.N., Savel'ev, D.P., and Savel'eva, O.L. (2010) Albian-cenomanian radiolarian assemblage from the Smaginsk formation, the Kamchatskii Mys Peninsula of Eastern Kamchatka. Stratigraphy and Geological Correlation, 18, 63-82.

Park, J.W., Hu, Z., Gao, S., Campbell, I.H., and Gong, H. (2012) Platinum group element abundances in the upper continental crust revisited - New constraints from analyses of Chinese loess. Geochimica et Cosmochimica Acta, 93, 63-76.

Patten, C., Barnes, S.J., and Mathez, E.A. (2012) Textural variations in MORB sulfide droplets due to differences in crystallization history. Canadian Mineralogist, 50, 675-692.

Patten, C., Barnes, S.J., Mathez, E.A., and Jenner, F.E. (2013) Partition coefficients of chalcophile elements between sulfide and silicate melts and the early crystallization history of sulfide liquid: LA-ICP-MS analysis of MORB sulfide droplets. Chemical Geology, 358, 170-188.

Peach, C.L., Mathez, E.A., and Keays, R.R. (1990) Sulfide melt-silicate melt distribution coefficients for noble metals and other chalcophile elements as deduced from MORB: Implication for partial melting. Geochimica et Cosmochimica Acta, 54, 3379-3389.

Portnyagin, M., Hoernle, K., and Savelyev, D. (2009) Ultra-depleted melts from Kamchatkan ophiolites: Evidence for the interaction of the Hawaiian plume with an oceanic spreading center in the Cretaceous? Earth and Planetary Science Letters, 287, 194-204.

Portnyagin, M., Savelyev, D., Hoernle, K., Hauff, F., and Garbe-Schonberg, D. (2008) Mid-Cretaceous Hawaiian tholeiites preserved in Kamchatka. Geology, 36, 903-906.

Portnyagin, M.V., Savel'ev, D.P., and Hoernle, K. (2005) Plume-related association of Cretaceous oceanic basalts of Eastern Kamchatka: Compositions of spinel and parental magmas. Petrology, 13, 571-588.

Roedder, E. (1992) Fluid inclusion evidence for immiscibility in magmatic differentiation. Geochimica et Cosmochimica Acta, 56, 5-20.

Saveliev, D.P. (2003) Intraplate alkali basalts in the Cretaceous accretionary complex of the Kamchatsky Peninsula (Eastern Kamchatka). Volcanology and Seismology, 1, 14-20 (in Russian).

Savelyev, D.P. (2014) Plagioclase picrites in the Kamchatsky Mys Peninsula, Eastern Kamchatka. Journal of Volcanology and Seismology, 8, 239-249.

Sylvester, P.J. (2001) A practical guide to platinum-group element analysis of sulphides by laser-ablation ICPMS. In P.J. Sylvester, Ed. Laser-ablation in the earth sciences: principles and application, 29, p. 203-213. Mineralogical Association of Canada.

Sylvester, P.J., Cabri, L.J., Tubrett, M.N., McMahon, G., Laflamme, J.H.G., and Peregoedova, A. (2005) Synthesis and evaluation of a fused pyrrhotite standard reference material for platinum group element and gold analysis by laser ablation-ICPMS. In T.O. Tormanen, and T.T. Alapieti, Eds. 10th International Platinum Symposium "Platinum Group Elements - from genesis to benefication and environmental impact", p. 16-20, Oulu, Finland.

Veksler, I.V., Dorfman, A.M., Dulski, P., Kamenetsky, V.S., Danyushevsky, L.V., Jeffries, T., and Dingwell, D.B. (2012) Partitioning of elements between silicate melt and immiscible

673 fluoride, chloride, carbonate, phosphate and sulfate melts with implications to the origin
674 of natrocarbonatite. Geochimica et Cosmochimica Acta, 79, 20-40.
675 Yang, A.Y., Zhou, M.-F., Zhao, T.-P., Deng, X.-G., Qi, L., and Xu, J.-F. (2014) Chalcophile
676 elemental compositions of MORBs from the ultraslow-spreading Southwest Indian Ridge
677 and controls of lithospheric structure on S-saturated differentiation. Chemical Geology,
678 382, 1-13.
679 Zelenski, M., Kamenetsky, V.S., and Hedenquist, J. (2016) Gold recycling and enrichment
680 beneath volcanoes: A case study of Tolbachik, Kamchatka. Earth and Planetary Science
681 Letters, 437, 35–46.
682 Zelenski, M., Kamenetsky, V.S., Mavrogenes, J.A., Danyushevsky, L.V., Matveev, D., and
683 Gurenko, A.A. (2017) Platinum-group elements and gold in sulfide melts from modern
684 arc basalt (Tolbachik volcano, Kamchatka). Lithos, 290-291, 172-188.
685 Zhang, Y. (2015) Toward a quantitative model for the formation of gravitational magmatic
686 sulfide deposits. Chemical Geology, 391, 56-73.

687

688 **FIGURE 1**. Schematic geological map of Kamchatsky Mys (modified after Savelyev, 2014)
689 showing location of studied rocks (star). (1-4) – sedimentary rocks of the Pliocene-Quaternary
690 (1), Miocene (2), Turonian-Campanian (3) and Albian–Cenomanian (4) ages. Early Cretaceous
691 ophiolite is represented by ultramafic rocks (5), gabbro and dolerites (6) and serpentinites
692 mélange (7). Geological boundaries are shown as faults (8) and thrusts (9).

693 **FIGURE 2**. Sulfides in the groundmass of Kamchatsky Mys picrites. Shapes of matrix sulfides (S)
694 vary from round to semi-spherical to cuspate and angular, depending on surrounding grains of
695 olivine (ol), Cr-spinel (sp), Ti-magnetite (mt), plagioclase (pl) and clinopyroxene (cpx). All
696 images are taken in backscattered electrons, except transmitted light in Fig. 2c.

697 **FIGURE 3**. Sulfides globules (S) in olivine (ol) phenocrysts. Globules, interpreted as sulfide melt
698 inclusions, are composed of Fe-rich, Ni poor phase, resembling pyrrhotite (*Fe-Mss*), Fe-Ni (*Mss*)
699 and Fe-Cu-Ni phase (*Iss*). Sulfide globules associate with inclusions of Cr-spinel (sp) and silicate
700 melt (MI). Hydrous silicate minerals (sr) replace olivine along numerous fractures.
701 Fragmentation of olivine by fractures and related alteration significantly reduce the number of
702 sulfide globules available for homogenization and subsequent analyses. Images are taken in plain
703 transmitted light (Fig. 3a) and backscattered electrons (Figs. 3b and 3c).

704 **FIGURE 4**. Daughter sulfides globules (S) in partially crystallized silicate melt inclusions hosted
705 by phenocrysts of olivine (ol, Figs. 4a–4c) and Cr-spinel (sp, Figs. 4d–4f). Apart from small
706 daughter sulfides (Figs. 4a, b and e), the melt inclusions contain daughter clinopyroxene (cpx),
707 vapor bubbles (b), residual silicate glass (G) and accidently trapped sulfide melts. The latter are
708 distinguished by larger size and non-spherical shapes (Figs. 4c and 4f). Images are taken in plain
709 transmitted light (Fig. 4a) and backscattered electrons (Figs. 4b–4f).

FIGURE 5. Compositional variability of sulfide globules (at%) in the Kamchatsky Mys picrites. Sulfide melt inclusions in olivine SMI (open circles), Table 2) are compared to matrix sulfides (Fe-Ni (*Mss*) and Fe-Cu-Ni (*Iss*) phases), analyzed by the electron microprobe (diamonds, Fig. 5a, Appendix 2[1]) and laser ablation ICPMS (triangles, Fig. 5b), daughter sulfide globules in Cr-spinel–hosted melt inclusions (Fig. 5c) and 22 individual sulfide globules in MORB glass ALV 526-1 (closed circles on Fig. 5a after Peach et al., 1990). Fig. 5b also shows the average matrix sulfide (av.MS, black circle) as analyzed by laser ablation ICPMS, and fields of *Mss* and *Iss* compositions, denoted by the electron microprobe data from Fig. 5a. Solitary daughter sulfides in melt inclusions are shown by crosses on Fig. 5c; all other symbols represent multiple (from 3 to 8) globules in single inclusions.

FIGURE 6. The compositions of homogenized sulfide melt inclusions, analyzed by SEM-EDS at exposed surfaces and by LA-ICPMS in volume (a) and their relationships with the host olivine forsterite content (b).

FIGURE 7. Time-resolved laser ablation signals (y axis, counts per second (cps)) recorded for selected elements (masses) in homogenized sulfide melt inclusions in olivine. The microphotographs show the appearance of sulfides in reflected light and their corresponding numbers, as per Table 2.

FIGURE 8. Reflected light microphotographs showing representative matrix sulfides composed of *Mss* and *Iss* and time-resolved laser ablation signals (y axis, counts per second (cps)) recorded for selected elements (masses) in these phases (see Appendix 3[1]). Note distinct Au- and Pd-rich phases in sulfides (see text and Fig. 12 for more details).

FIGURE 9. Relationships between Co and chalcophile elements (Ni, Cd, and Zn) in the matrix sulfides and sulfide melt inclusions. Note that Co and Ni may have siderophile and chalcophile affinities.

FIGURE 10. Relationships between the noble metal (PGE, Au) contents in the matrix sulfides and sulfide melt inclusions.

FIGURE 11. Primitive mantle (after McDonough and Sun, 1995) – normalized concentrations of noble metals in (a) individual sulfide melt inclusions and (b) two Kamchatsky Mys picrites, compared to average sulfide melt inclusion (av.SMI) and average matrix sulfide (av.MS) compositions. For comparison, the PGE abundances in the rocks are increased by a factor of 10^3, based on estimated amounts of matrix sulfide (~ 0.1%, see text for details). Analytical precision (2σ) for individual analyses is shown as bars on Fig. 10a.

FIGURE 12. Backscattered electron images showing noble metal "nuggets" (circled) of dominantly Pd-Sn and Au-Ag compositions in matrix sulfides.

744 **FIGURE 13**. Backscattered electron images showing phases containing $PtAs_2$, Au –Ag and Ni
745 arsenides in fractures within matrix sulfides (Figs. 12a–12c), and in surrounding alteration-
746 related hydrous silicates (Figs. 12b–12d).

747 **FIGURE 14**. Relationships between the noble metal ratios in sulfide melt inclusions (open circles)
748 and their Ni/Cu (at.) and host olivine composition (Fo). The average matrix sulfide is shown with
749 closed circle.

This is a preprint, the final version is subject to change, of the American Mineralogist (MSA)
Cite as Authors (Year) Title. American Mineralogist, in press.
DOI: https://doi.org/10.2138/am-2018-6352

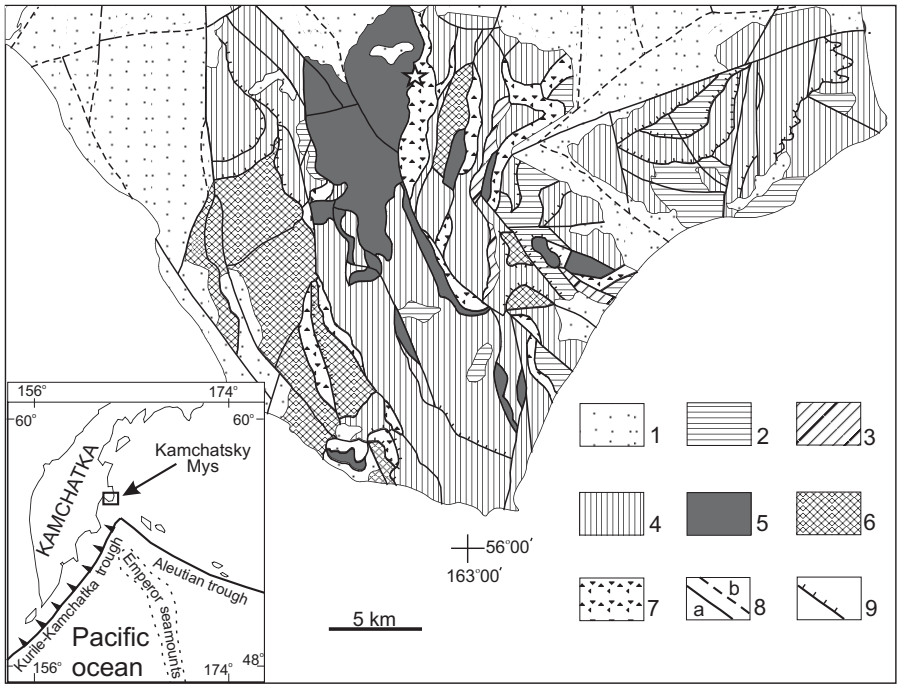

Fig. 1

This is a preprint, the final version is subject to change, of the American Mineralogist (MSA)
Cite as Authors (Year) Title. American Mineralogist, in press.
DOI: https://doi.org/10.2138/am-2018-6352

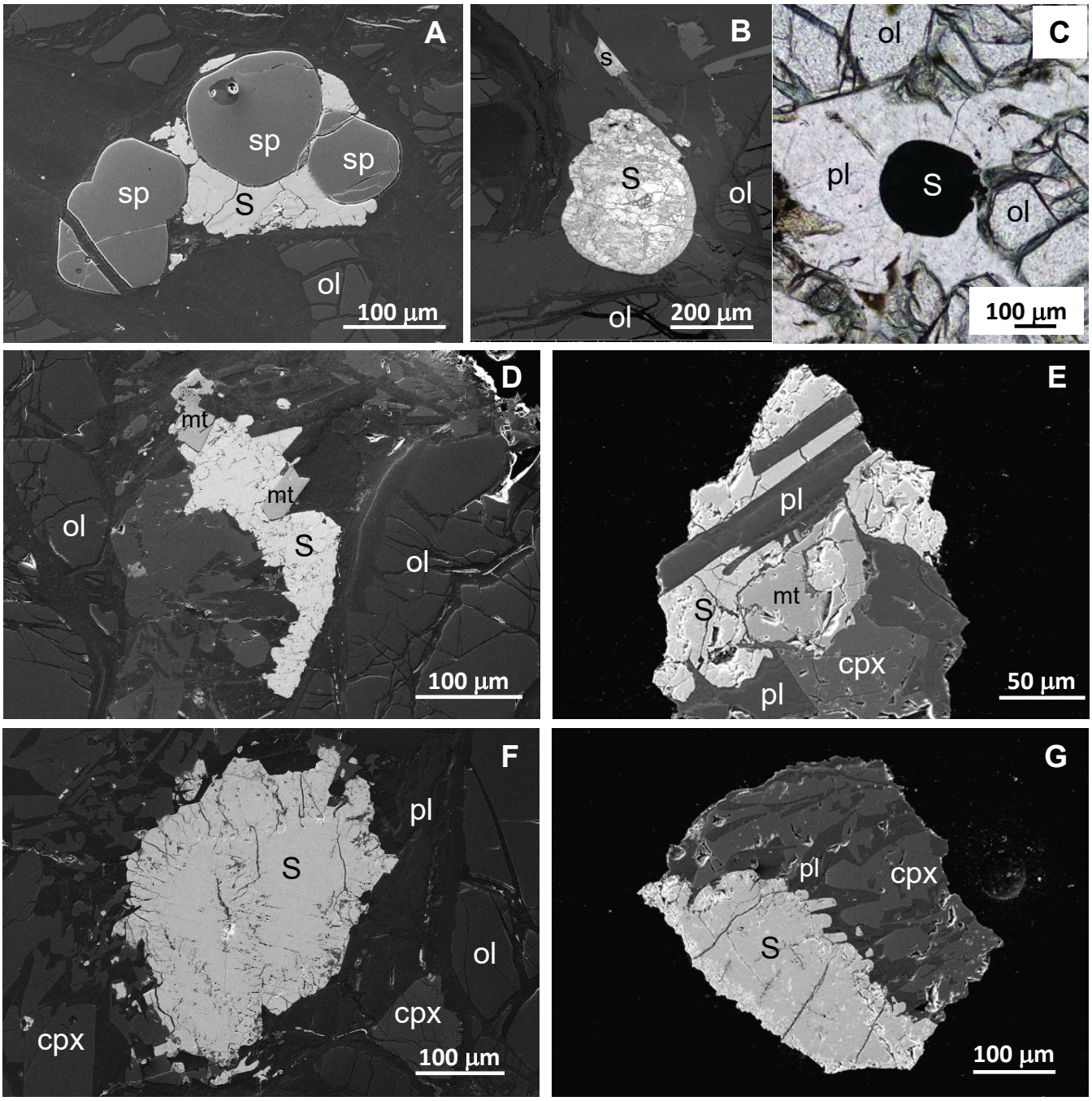

Fig. 2.

This is a preprint, the final version is subject to change, of the American Mineralogist (MSA)
Cite as Authors (Year) Title. American Mineralogist, in press.
DOI: https://doi.org/10.2138/am-2018-6352

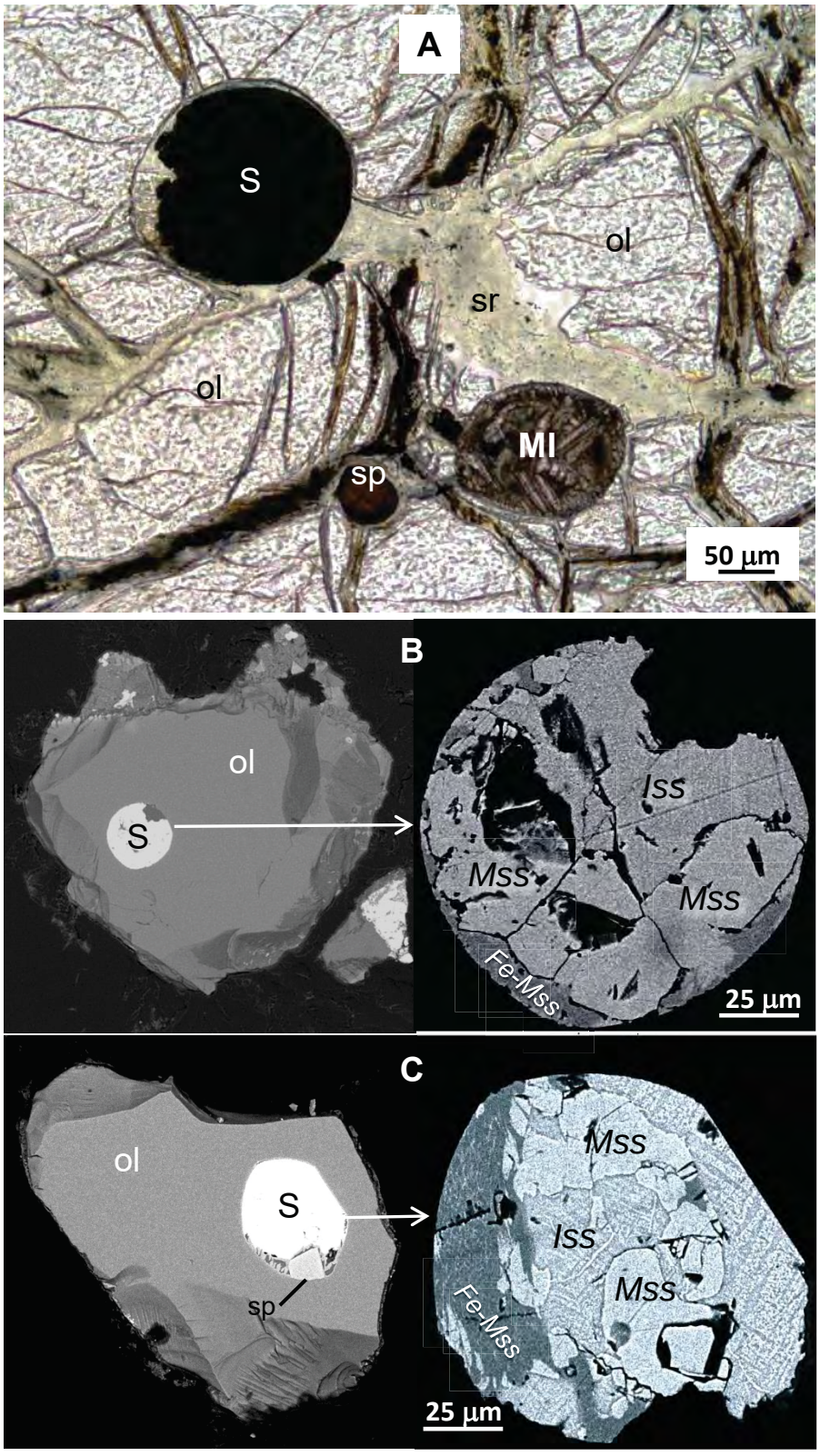

Fig. 3.

This is a preprint, the final version is subject to change, of the American Mineralogist (MSA)
Cite as Authors (Year) Title. American Mineralogist, in press.
DOI: https://doi.org/10.2138/am-2018-6352

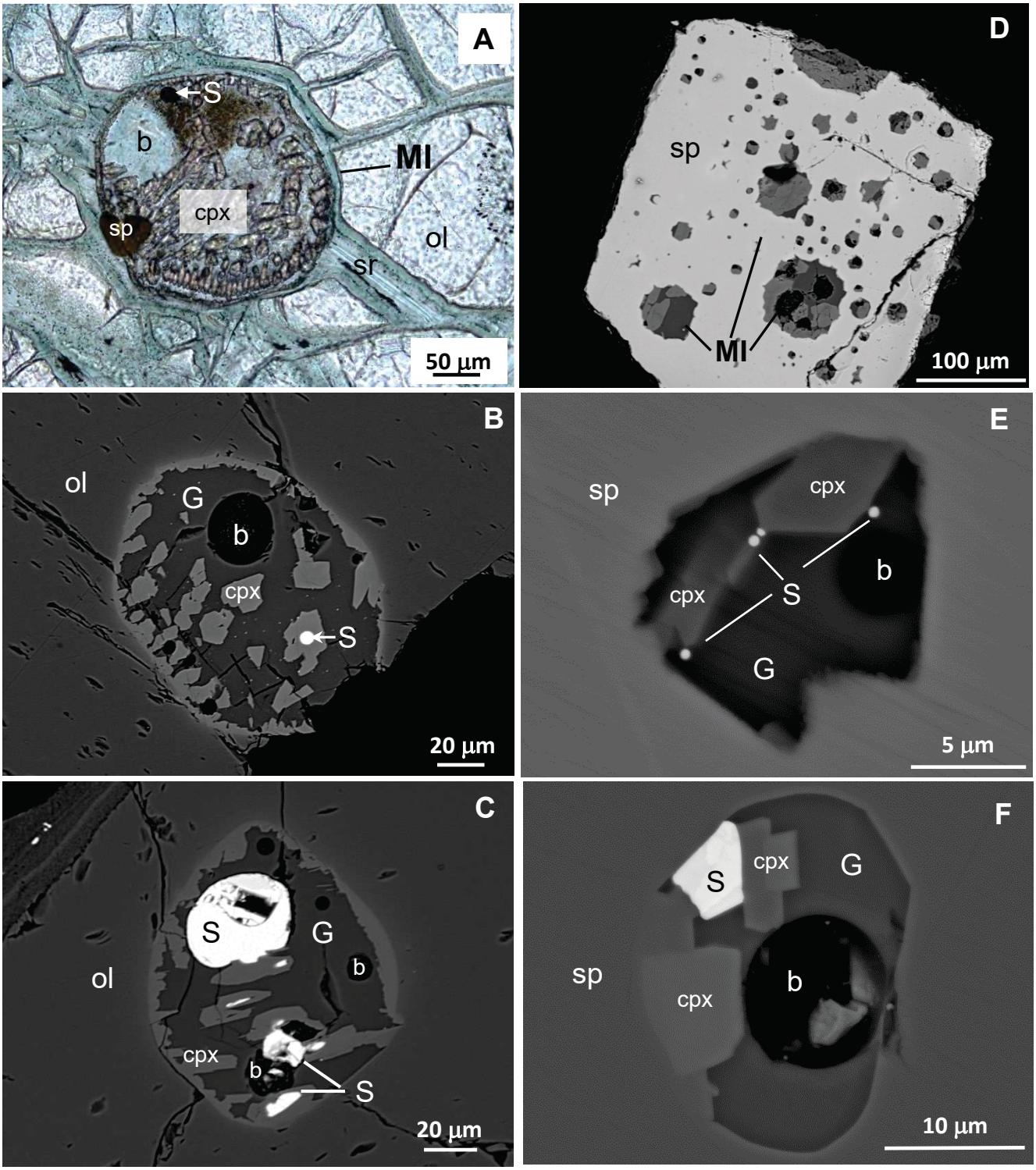

Fig. 4.

This is a preprint, the final version is subject to change, of the American Mineralogist (MSA)
Cite as Authors (Year) Title. American Mineralogist, in press.
DOI: https://doi.org/10.2138/am-2018-6352

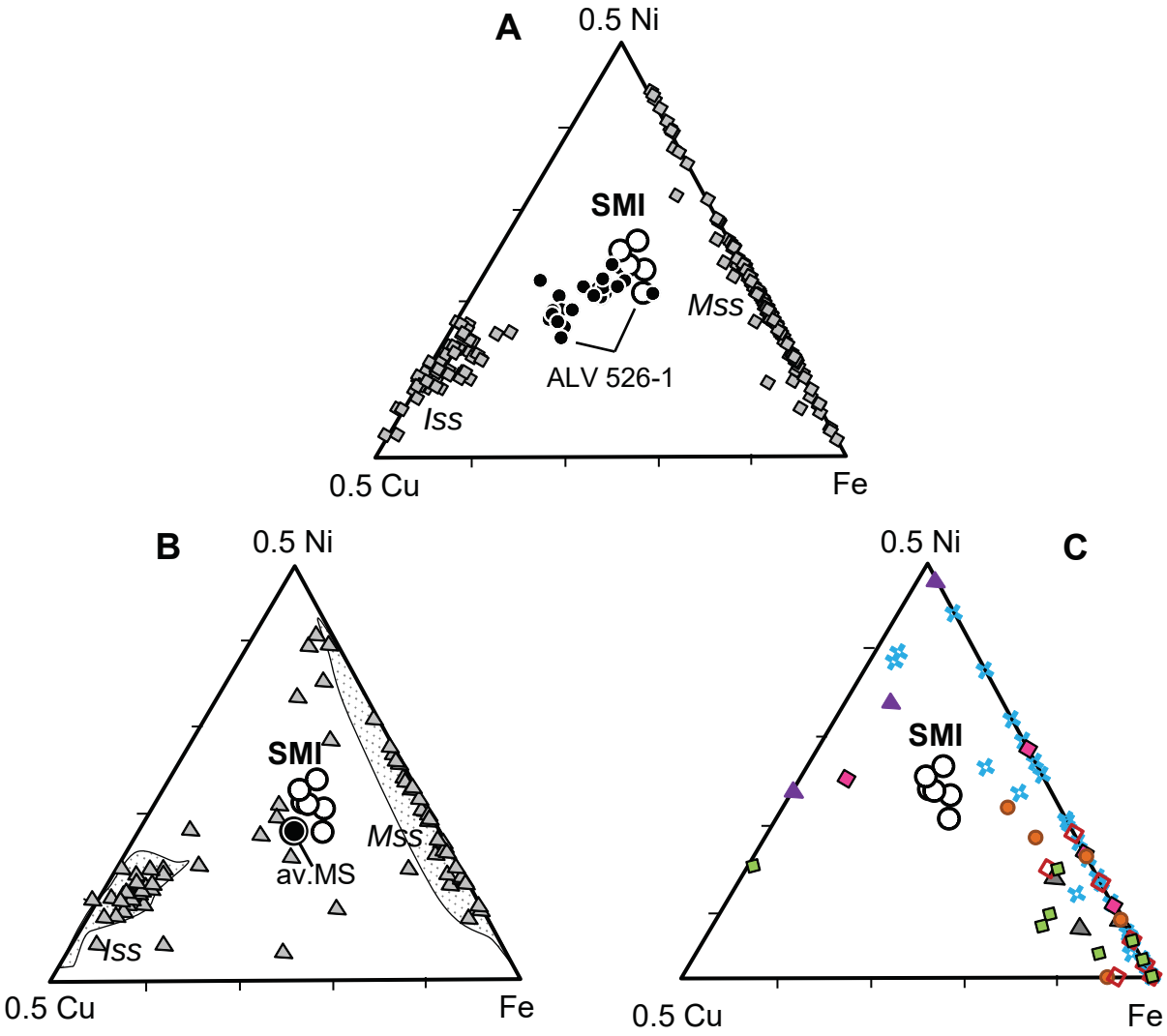

Fig. 5.

This is a preprint, the final version is subject to change, of the American Mineralogist (MSA)
Cite as Authors (Year) Title. American Mineralogist, in press.
DOI: https://doi.org/10.2138/am-2018-6352

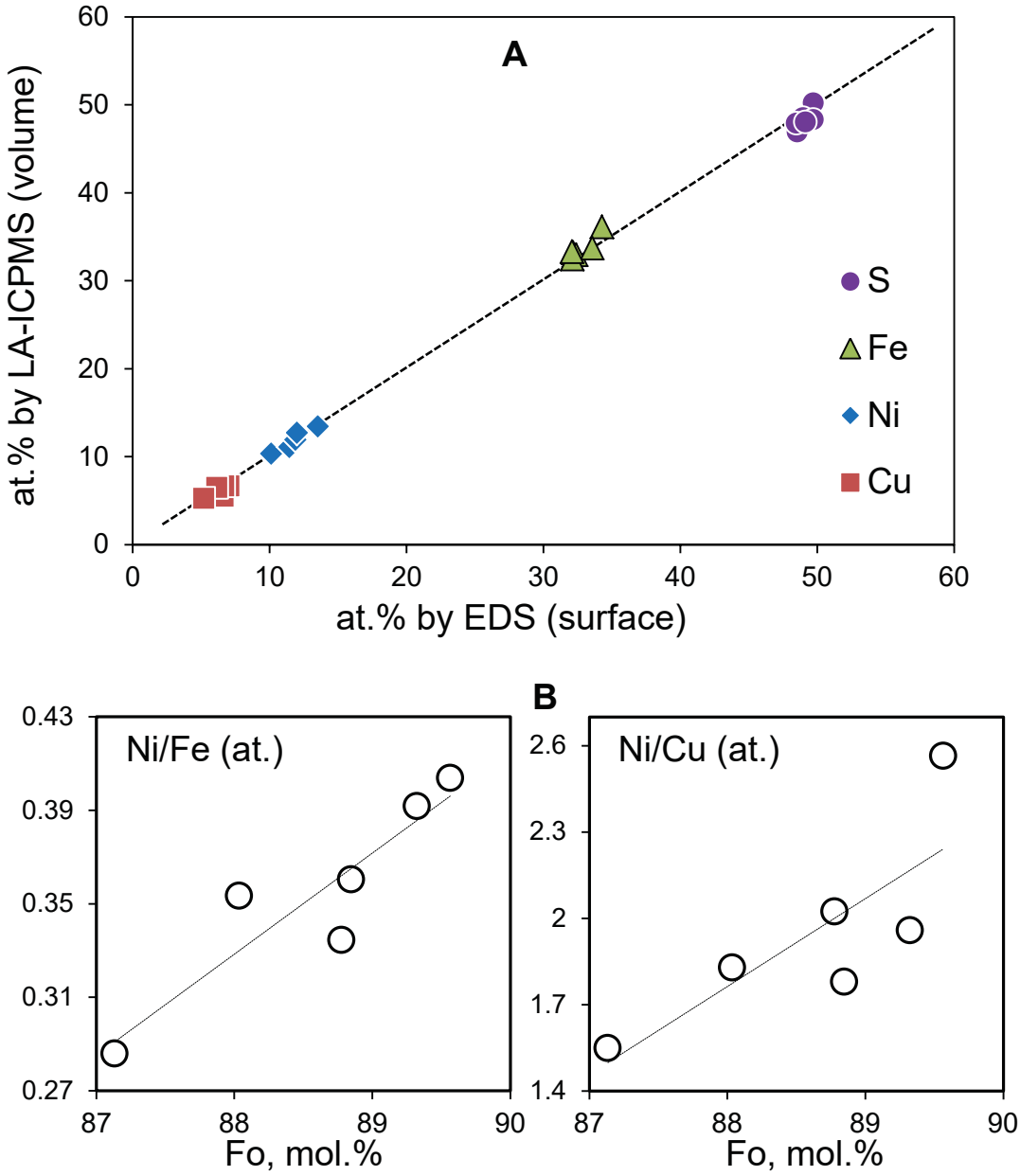

Fig. 6.

This is a preprint, the final version is subject to change, of the American Mineralogist (MSA)
Cite as Authors (Year) Title. American Mineralogist, in press.
DOI: https://doi.org/10.2138/am-2018-6352

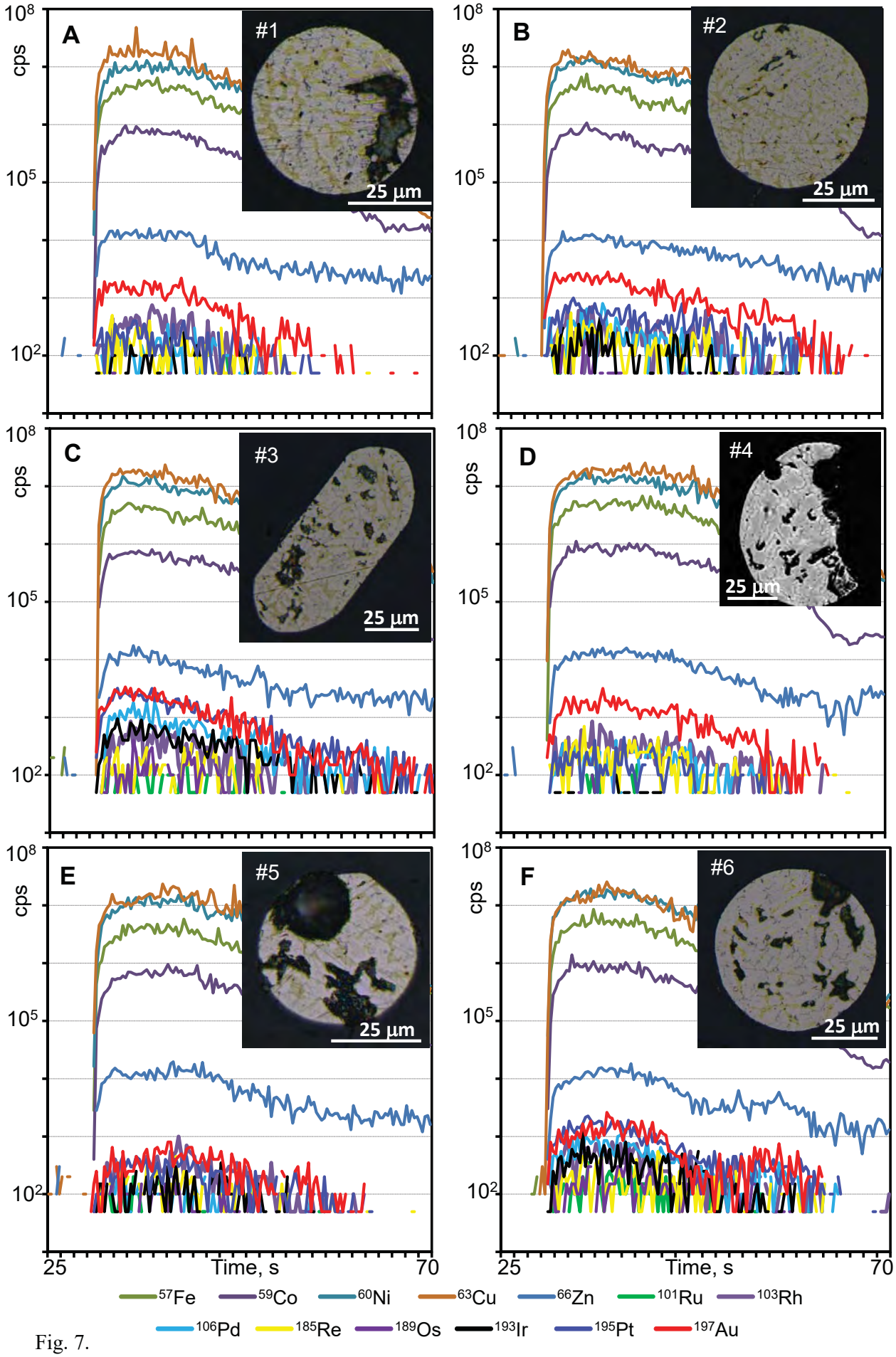

Fig. 7.

This is a preprint, the final version is subject to change, of the American Mineralogist (MSA)
Cite as Authors (Year) Title. American Mineralogist, in press.
DOI: https://doi.org/10.2138/am-2018-6352

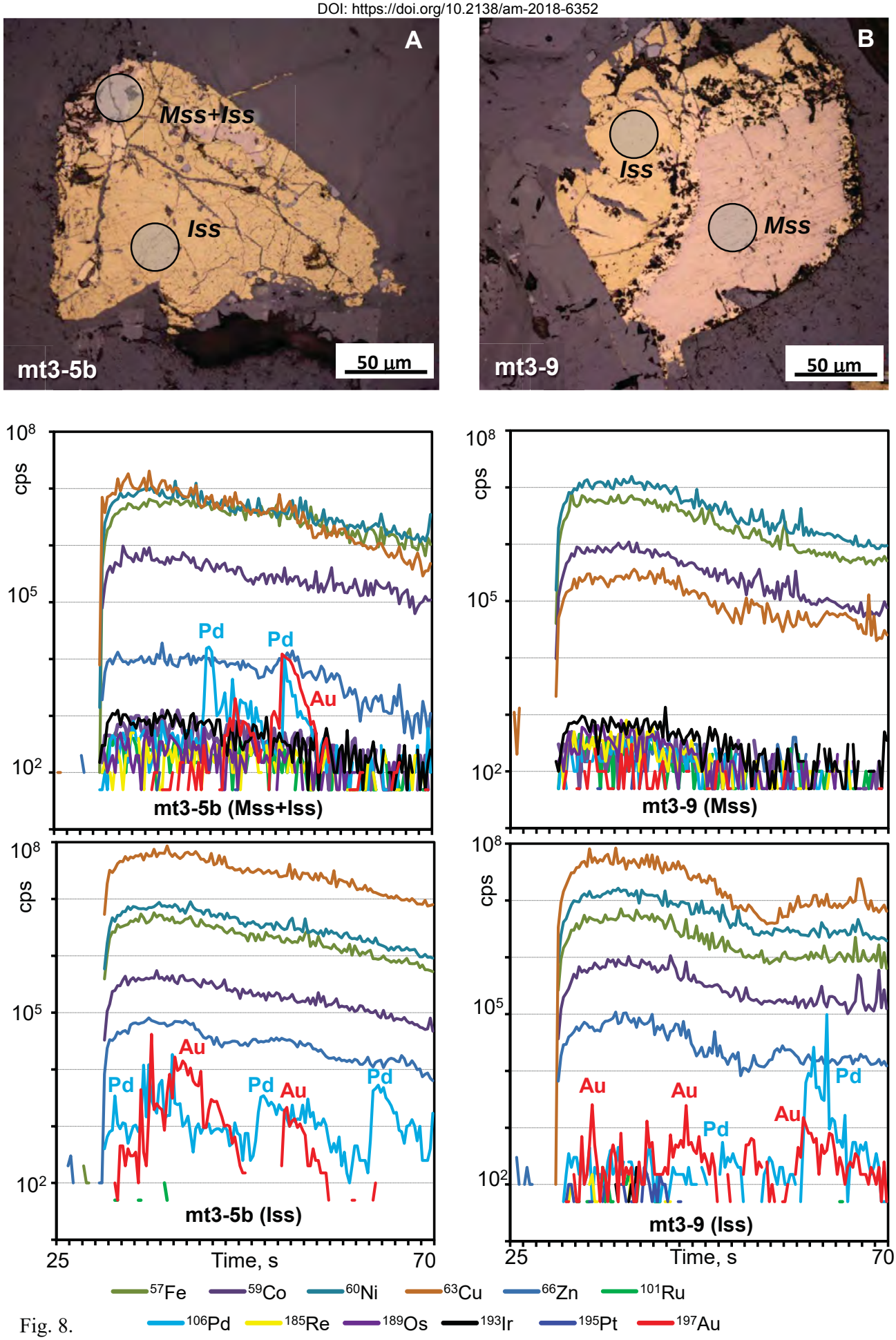

Fig. 8.

This is a preprint, the final version is subject to change, of the American Mineralogist (MSA)
Cite as Authors (Year) Title. American Mineralogist, in press.
DOI: https://doi.org/10.2138/am-2018-6352

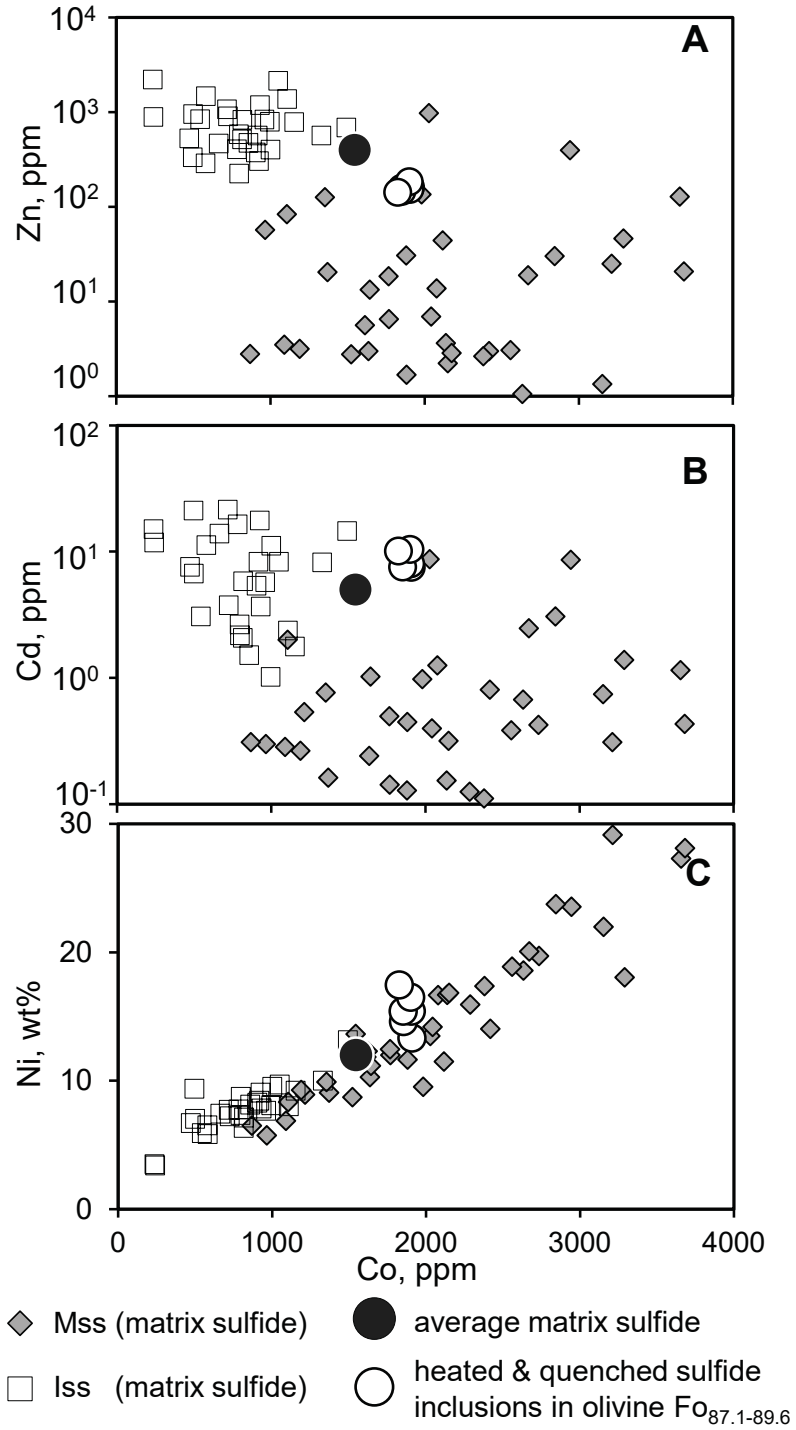

Fig. 9.

This is a preprint, the final version is subject to change, of the American Mineralogist (MSA)
Cite as Authors (Year) Title. American Mineralogist, in press.
DOI: https://doi.org/10.2138/am-2018-6352

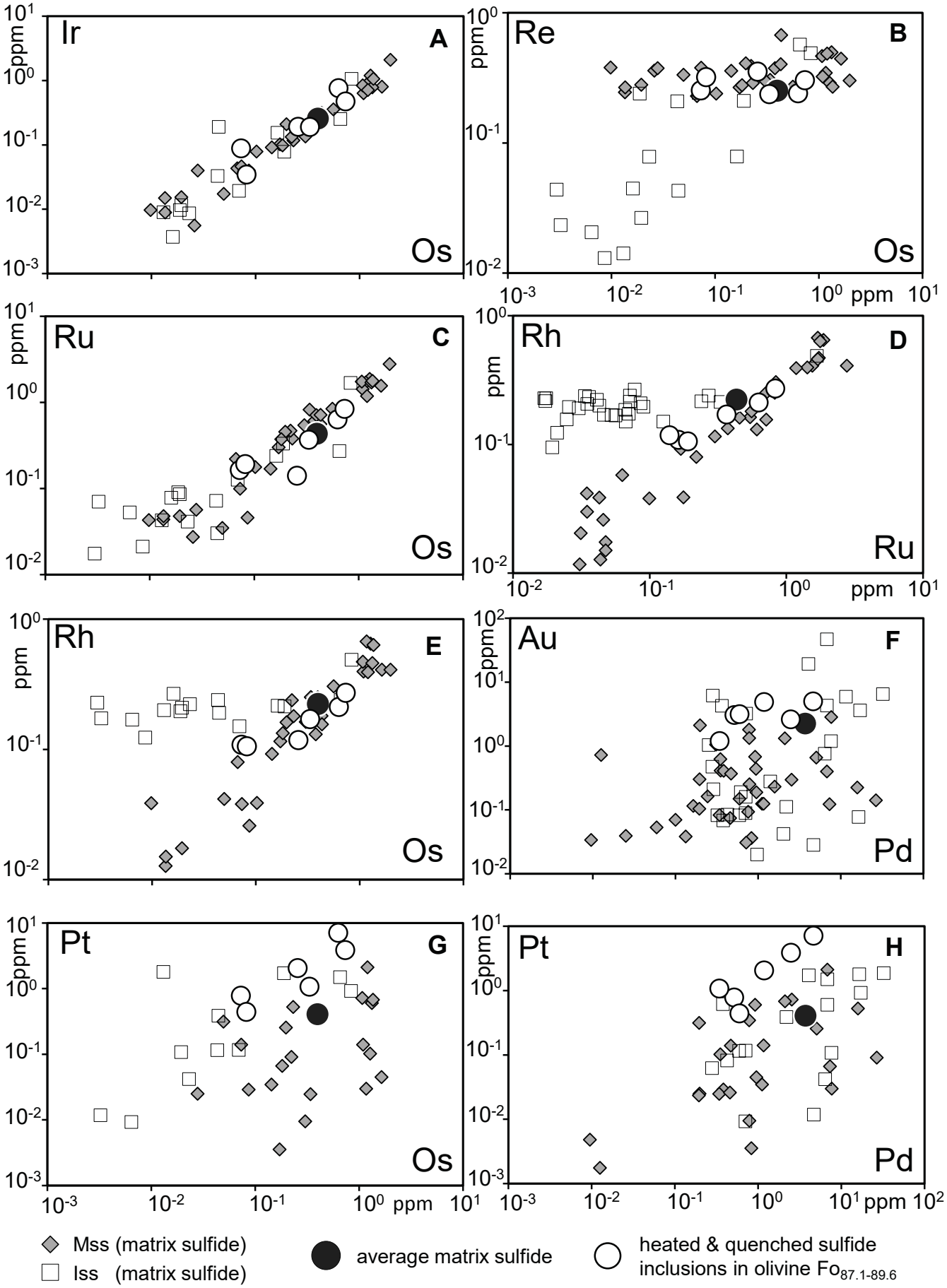

Fig. 10.

This is a preprint, the final version is subject to change, of the American Mineralogist (MSA)
Cite as Authors (Year) Title. American Mineralogist, in press.
DOI: https://doi.org/10.2138/am-2018-6352

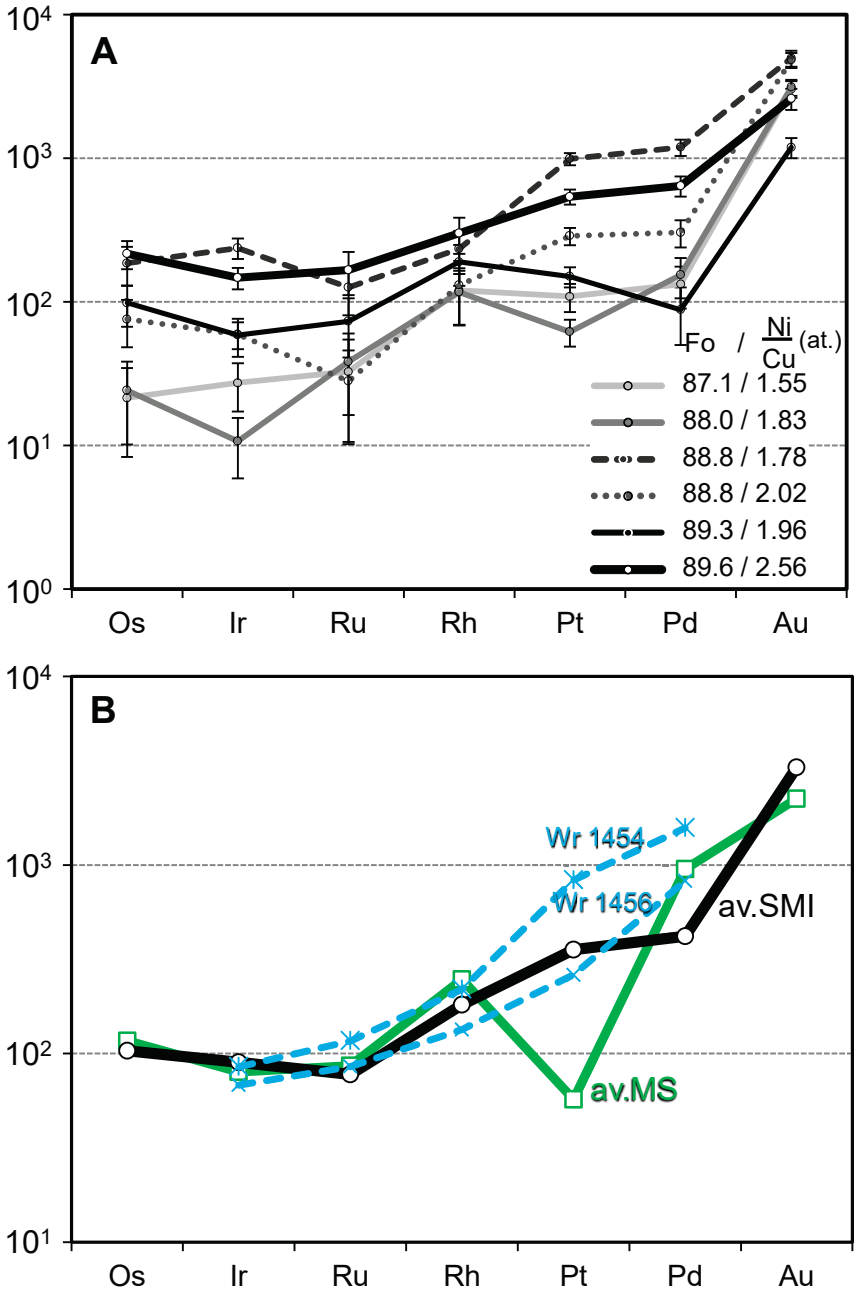

Fig. 11.

This is a preprint, the final version is subject to change, of the American Mineralogist (MSA)
Cite as Authors (Year) Title. American Mineralogist, in press.
DOI: https://doi.org/10.2138/am-2018-6352

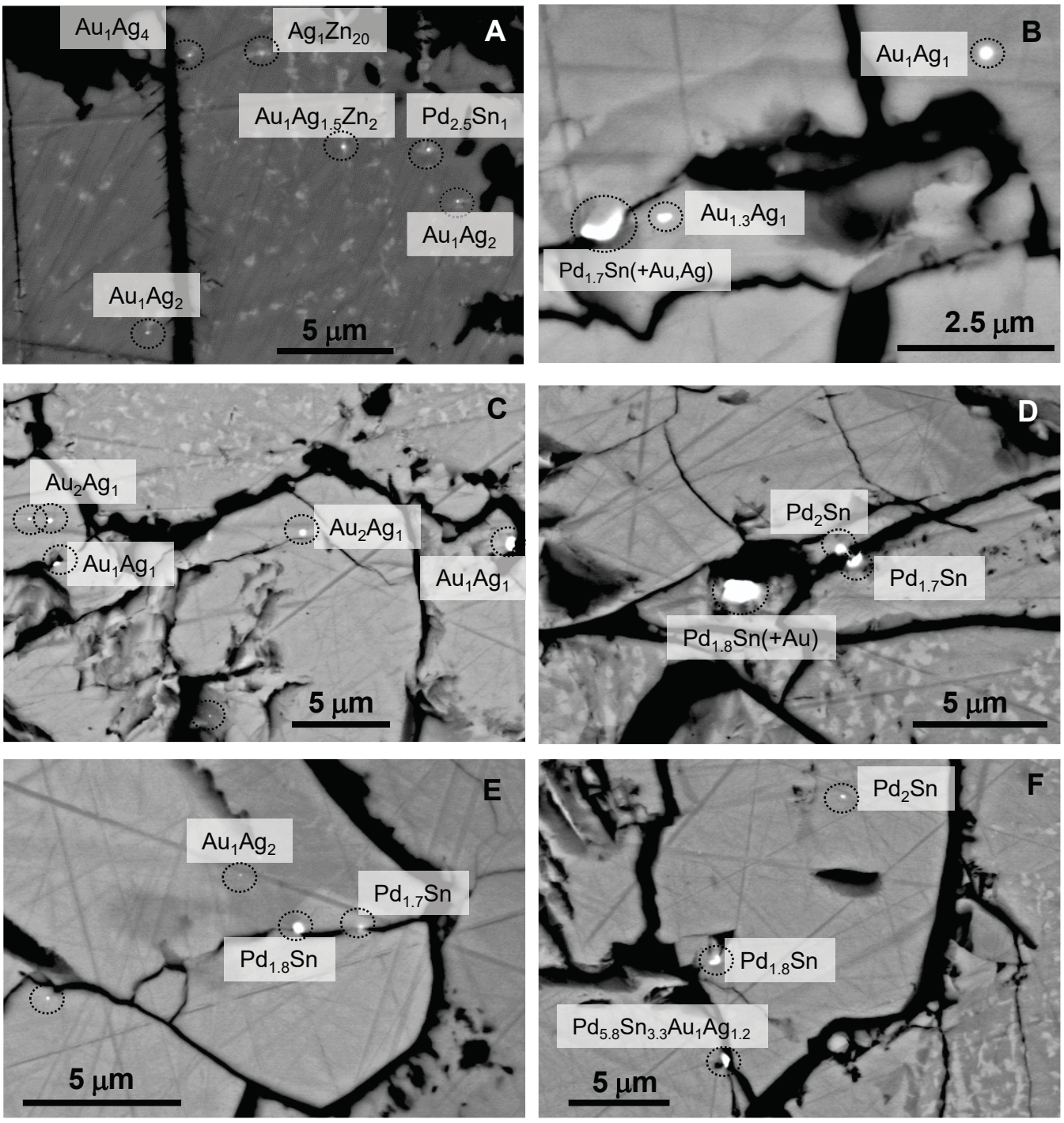

Fig. 12.

This is a preprint, the final version is subject to change, of the American Mineralogist (MSA)
Cite as Authors (Year) Title. American Mineralogist, in press.
DOI: https://doi.org/10.2138/am-2018-6352

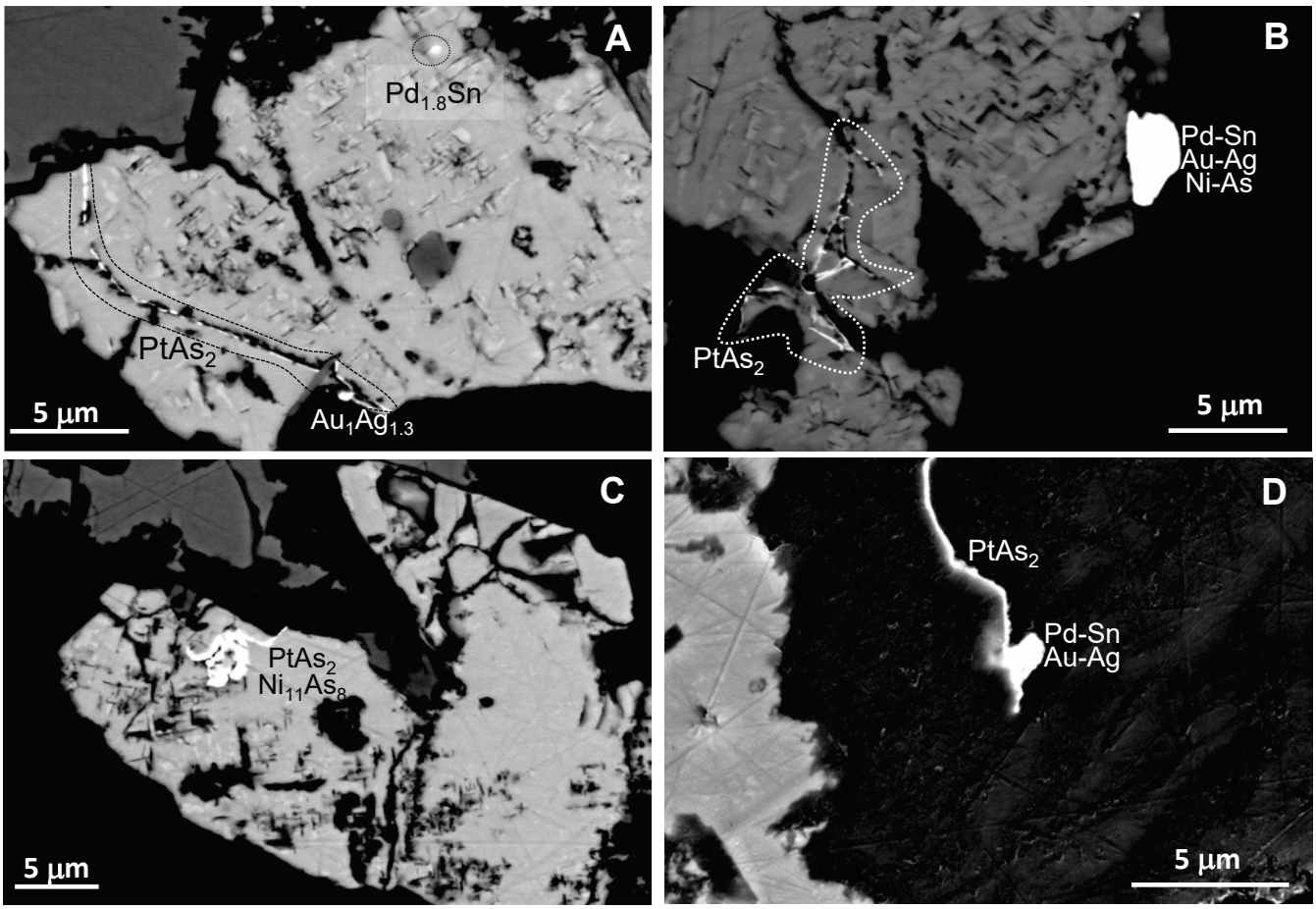

Fig. 13.

This is a preprint, the final version is subject to change, of the American Mineralogist (MSA)
Cite as Authors (Year) Title. American Mineralogist, in press.
DOI: https://doi.org/10.2138/am-2018-6352

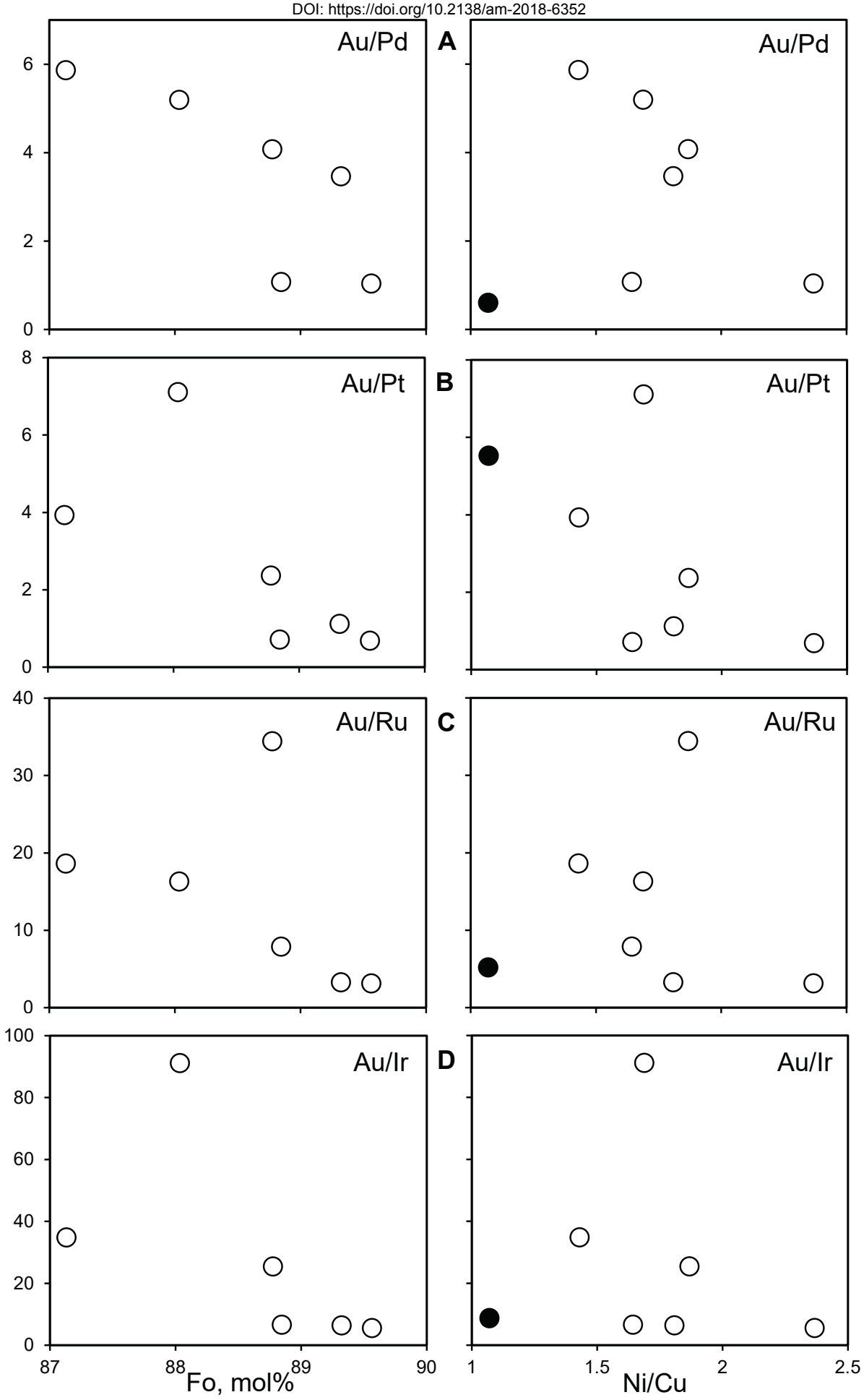

This is a preprint, the final version is subject to change, of the American Mineralogist (MSA)
Cite as Authors (Year) Title. American Mineralogist, in press.
DOI: https://doi.org/10.2138/am-2018-6352

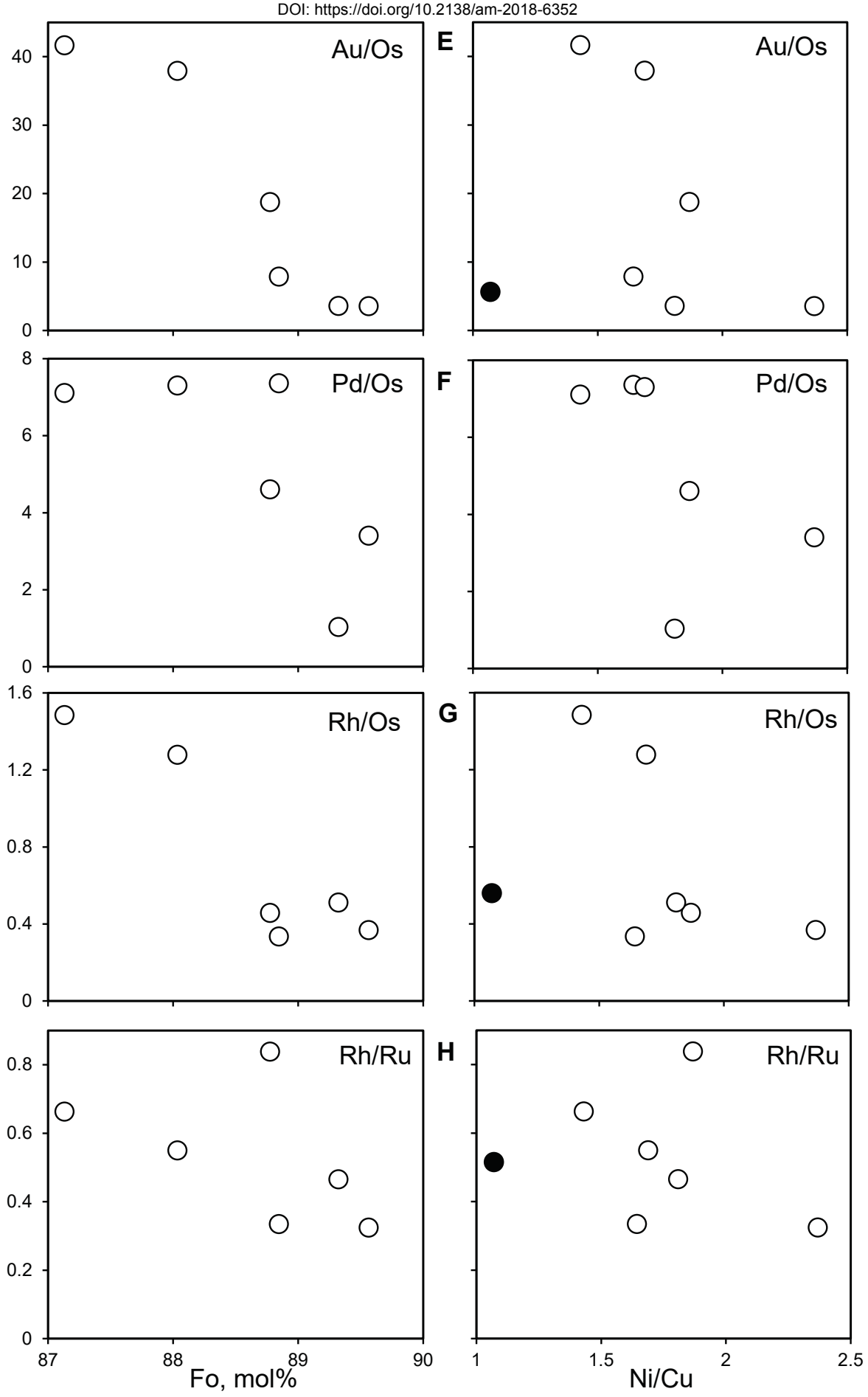

Fig. 14.

This is a preprint, the final version is subject to change, of the American Mineralogist (MSA)
Cite as Authors (Year) Title. American Mineralogist, in press.
DOI: https://doi.org/10.2138/am-2018-6352

Table 1. Compositions of sulfide-bearing olivine-phyric rocks from the Kamchatsky Mys, eastern Kamchatka

Sample	D1454-1	D1456-1		1454-1	1456-1		1454-1	1456-1
wt.%			ppm			ppb		
SiO_2	43.02	45.21	Sc	21.8	23.4	Ir	0.27	0.22
TiO_2	0.40	0.45	V	110	121	σ	0.01	0.01
Al_2O_3	7.89	8.84	Cr	1372	1185	Ru	0.58	0.43
Fe_2O_3	11.05	9.96	Co	102	102	σ	0.01	0.01
MnO	0.16	0.15	Ni	1252	1249	Rh	0.20	0.12
MgO	28.05	25.77	Cu	66.4	70.9	σ	0.01	0.00
CaO	5.47	5.54	Zn	54.8	62.1	Pt	5.91	1.85
Na_2O	0.85	0.88	Y	7.2	8.0	σ	0.14	0.04
K_2O	0.04	0.04	Zr	21.4	24.1	Pd	6.13	3.21
P_2O_5	0.04	0.04	Nb	1.8	2.0	σ	0.20	0.15
S	0.04	0.06	La	1.4	1.6			
LOI	3.00	3.06	Gd	1.08	1.24			
Total	100.01	100.00	Yb	0.81	0.90			

This is a preprint, the final version is subject to change, of the American Mineralogist (MSA)
Cite as Authors (Year) Title. American Mineralogist, in press.
DOI: https://doi.org/10.2138/am-2018-6352

Table 2. Compositions of homogenized sulfide melt inclusions and average *Mss* and *Iss* phases matrix sulfides analyzed by LA-ICPMS

	1	**2**	**3**	**4**	**5**	**6**	**7**	**8**
S, wt.%	33.0	36.0	34.4	33.8	34.2	34.0	35.21	34.31
Fe, wt.%	44.2	41.5	40.7	41.5	40.0	41.1	48.52	32.48
Ni, wt.%	13.3	14.6	15.4	15.4	16.5	17.4	15.32	7.75
Cu, wt.%	9.3	7.8	9.4	9.1	9.1	7.4	0.75	25.38
(Fe+Ni+Cu)/S, at.	1.13	0.99	1.06	1.09	1.07	1.08	1.04	1.04
Co, ppm	1911	1854	1906	1853	1901	1827	2081	807
Zn, ppm	159	156	151	144	182	141	61.87	789
Cd, ppm	7.44	9.25	7.94	7.49	10.33	10.03	1.10	9.37
Re, ppm	0.25	0.35	0.24	0.32	0.24	0.30	0.34	0.12
Os, ppm	0.07	0.26	0.63	0.08	0.33	0.74	0.50	0.13
Ir, ppm	0.09	0.19	0.76	0.03	0.19	0.47	0.32	0.10
Ru, ppm	0.16	0.14	0.63	0.19	0.37	0.83	0.60	0.13
Rh, ppm	0.11	0.12	0.21	0.11	0.17	0.27	0.21	0.21
Pt, ppm	0.77	2.04	7.03	0.44	1.06	3.82	0.24	0.62
Pd, ppm	0.52	1.19	4.64	0.60	0.34	2.50	2.25	4.40
Au, ppm	3.03	4.83	4.96	3.12	1.19	2.60	0.46	3.87
Host olivine (Fo, mol.%)	87.1	88.8	88.8	88.0	89.3	89.6		

Analyses of homogenized melt inclusions in olivine, labelled from 1 to 6, correspond to images and time-resolved laser ablation spectra on Figs. 7a–7f. Compositions 7 and 8 represent average Mss (n=40) and Iss (n=29), respectively, in matrix sulfides.